The Geological Society of America
Special Paper 446
2008

Magnetostratigraphy of the eastern Hadar Basin (Ledi-Geraru research area, Ethiopia) and implications for hominin paleoenvironments

Guillaume Dupont-Nivet*
Faculty of Geosciences, Paleomagnetic Laboratory "Fort Hoofddijk," Utrecht University, Budapestlaan 17, 3584 CD Utrecht, The Netherlands

Mark Sier
Faculty of Geosciences, Paleomagnetic Laboratory "Fort Hoofddijk," Utrecht University, Budapestlaan 17, 3584 CD Utrecht, The Netherlands, and *Faculty of Archaeology, Leiden University, P.O. Box 9515, 2300 RA Leiden, The Netherlands*

Christopher J. Campisano
Institute of Human Origins, School of Human Evolution and Social Change, Arizona State University, P.O. Box 874101, Tempe, Arizona 85287-4101, USA

J Ramón Arrowsmith
Erin DiMaggio
School of Earth and Space Exploration, Arizona State University, Tempe, Arizona 85287-1404, USA

Kaye Reed
Institute of Human Origins, School of Human Evolution and Social Change, Arizona State University, P.O. Box 874101, Tempe, Arizona 85287-4101, USA

Charles Lockwood†
Department of Anthropology, University College London, Gower Street, London WC1E 6BT, UK

Christine Franke§
Faculty of Geosciences (FB 5), University of Bremen, P.O. Box 330440, D-28334 Bremen, Germany

Silja Hüsing
Faculty of Geosciences, Paleomagnetic Laboratory "Fort Hoofddijk," Utrecht University, Budapestlaan 17, 3584 CD Utrecht, The Netherlands

THIS PAPER IS DEDICATED TO THE MEMORY OF CHARLES LOCKWOOD.

*Corresponding author: gdn@geo.uu.nl.
†Deceased.
§Current address: Laboratoire des Sciences du Climat et de l'Environnement, Avenue de la Terrasse, Bat. 12, F-91198 Gif-sur-Yvette Cedex, France.

Dupont-Nivet, G., Sier, M., Campisano, C.J., Arrowsmith, J R., DiMaggio, E., Reed, K., Lockwood, C., Franke, C., and Hüsing, S., 2008, Magnetostratigraphy of the eastern Hadar Basin (Ledi-Geraru research area, Ethiopia) and implications for hominin paleoenvironments, *in* Quade, J., and Wynn, J.G., eds., The Geology of Early Humans in the Horn of Africa: Geological Society of America Special Paper 446, p. 67–85, doi: 10.1130/2008.2446(03).

ABSTRACT

To date and characterize depositional environments of the hominin-bearing Hadar Formation, lacustrine sediments from the eastern part of the Hadar Basin (Ledi-Geraru research area) were studied using tephrostratigraphy and magnetostratigraphy. The Sidi Hakoma Tuff, Triple Tuff-4, and the Kada Hadar Tuff, previously dated by $^{40}Ar/^{39}Ar$ in other parts of the basin, were identified using characteristic geochemical composition and lithologic features. Paleomagnetic samples were collected every 0.5 m along an ~230-m-thick composite section between the Sidi Hakoma Tuff and the Kada Hadar Tuff. A primary detrital remanent magnetization mostly carried by (titano-) magnetites of basaltic origin was recognized. Consistent with existing data of the Hadar Basin, paleomagnetic directions show a postdepositional counterclockwise vertical-axis tectonic rotation (~5°–10°) and shallowing of paleomagnetic inclination (~5°–10°) related to sedimentation and compaction. Two normal-polarity intervals (chrons 2An.3n and 2An.2n) are recorded bracketing a reversed interval identified as the Mammoth event (chron 2An.2r). Resulting sediment accumulation rates (~90 cm/k.y.) are high compared to existing accumulation-rate estimates from the more western part of the Hadar Basin. The resulting eastward increasing trend suggests that deposition took place in an eastward-tilting basin. Sediment accumulations were constant throughout the basin from ca. 3.4 to 3.2 Ma. At 3.2 Ma, a regional and relatively short-lived event is indicated by significant change in depositional conditions and a large increase in accumulation rate. This disruption may have been related to increased climate variability due to astronomical climate forcing. It provides a possible explanation for changes in the Hadar faunal community and *Australopithecus afarensis* in particular.

Keywords: magnetostratigraphy, tephrostratigraphy, paleoanthropology, paleoenvironment, Pliocene, East African Rift.

INTRODUCTION

To understand how past environments may have influenced hominin evolution, temporal and causal relationships must be established between records of paleoenvironmental changes and the hominin fossil record. Recent advances arise from climate modeling and the availability of well-calibrated regional paleoclimatic records (deMenocal, 2004; Sepulchre et al., 2006), but accurately dated analysis of hominin-bearing sediments is needed to place fossils in their tectonic and climatic context. The Pliocene Hadar Basin in the Afar region of northern Ethiopia (Fig. 1) includes some of the world's most complete collections of hominins (Johanson and Taieb, 1976; Johanson et al., 1982; Kimbel et al., 2004; Alemseged et al., 2006). As a result, sediments of the Hadar Basin have been studied intensively since the 1970s. Successful dating has been achieved using the combination of radiochronologic methods (mainly $^{40}Ar/^{39}Ar$) on interlayered volcanic deposits and magnetostratigraphy (Aronson et al., 1977; Schmitt and Nairn, 1984; Renne et al., 1993; Tamrat et al., 1996; Walter and Aronson, 1993; Walter, 1994). Understandably, most geological work (e.g., Campisano and Feibel, this volume, and references therein) has focused on regions with high densities of fossil finds in the Hadar research area (Fig. 1). However, geologic work over the entire Hadar Basin is needed to fully constrain its paleoenvironment. The Dikika research area south of the Awash River and the Gona research area west of Hadar have been recently examined extensively (Quade et al., 2004, this volume; Wynn et al., 2006; Wynn et al., this volume). In the present study, we investigate and date the stratigraphy from a still poorly explored region of the eastern Hadar Basin that is referred to as the Ledi-Geraru research area, initially documented by the International Afar Research Expedition in the 1970s. The Ledi-Geraru area, east of the Hurda (= Ourda) wadi and north of the Awash River, provides the opportunity to better constrain the Hadar Basin history in space and time and to assess if environmental changes observed in other research areas are indeed regional and not related to local disturbance from faults, hiatuses, or variations in sediment accumulation. We present chronology of this previously undated stratigraphy using magnetostratigraphic analysis along with correlation of tuffaceous horizons found in the Ledi-Geraru area to their radiochronologically dated counterparts in the Hadar Formation. The results enable us to place paleontological finds in a well-calibrated chronostratigraphic framework and increase our understanding of the tectonic and climatic conditions that prevailed during their deposition.

GEOLOGICAL SETTING

Regional Geologic Setting

The Hadar Basin formed as an extensional subbasin of the subsiding Afar Depression at the triple junction of the Ethiopian Rift, the Aden Rift, and the Red Sea Rift (Fig. 1). Exposures of

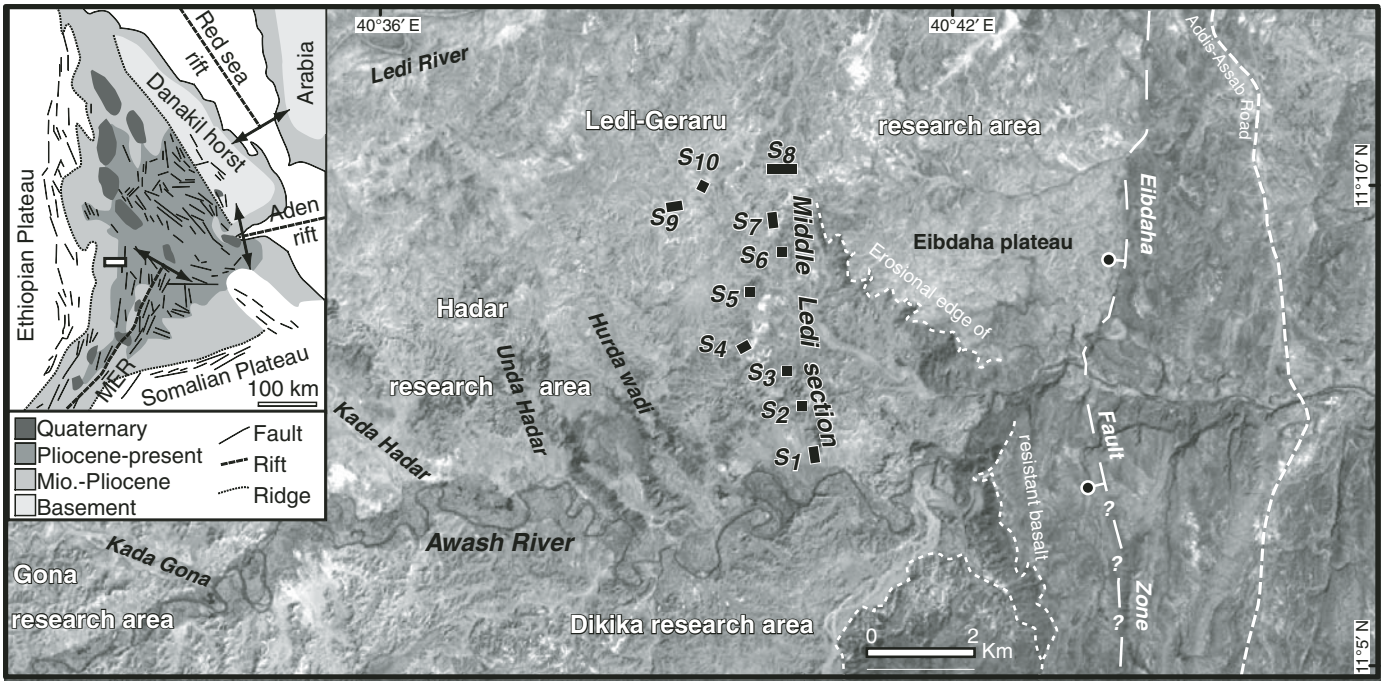

Figure 1. Locations of the subsections of the Middle Ledi section sampled for magnetostratigraphy (S_1–S_{10}) within the Ledi-Geraru research area. Map is overlain on grayscale version of Advanced Spaceborne Thermal Emission and Reflection Radiometer (ASTER) imagery and Shuttle Radar Topography Mission (SRTM) imagery. The Eibdaha fault zone delineation is based on field observations, analysis of 90 m digital elevation models (SRTM), and stereo aerial photography. Inset shows location of sampling area (white box) in the tectonic context of the Afar triple junction (simplified from Thurmond et al., 2006). MER—Main Ethiopian Rift.

the Hadar Formation defining the Hadar Basin are located along the Ethiopian Rift margin, just east of the Ethiopian escarpment, which separates the Afar Depression from the Ethiopian Plateau. The Ethiopian Plateau, probably present since the Oligocene (Pik et al., 2003), controls eastward river flow into the Afar Depression (in particular, the Awash River) but also northward flow into the Mediterranean through the Nile River. Atmospheric circulation modeling shows that the plateau obstructs zonal circulation and deflects Indian monsoon flow, such that enhanced Miocene-Pliocene uplift possibly induced aridification and environmental change in East Africa (Sepulchre et al., 2006; Gani et al., 2007; Spiegel et al., 2007). Rifting and subsidence of the Afar Depression commenced after the Oligocene (Ukstins et al., 2002). The most activity has occurred since 20 Ma, when the Gulf of Aden Rift joined the triple junction, driving widespread volcanism, faulting, and rotations of crustal blocks (Acton et al., 2000; Manighetti et al., 2001; Audin et al., 2004). Alternatively, it has been proposed that the Main Ethiopian Rift, propagating from the southwest, reached the Afar Depression and connected to the triple junction only 11 m.y. ago (Wolfenden et al., 2004). Plate kinematic and crustal thickness reconstructions of the Afar suggest that, although stretching rates remained constant, regional subsidence in the Hadar block was virtually complete by mid-Pliocene time (Redfield et al., 2003). Sustained deformation and volcanic activity during Pliocene time possibly shifted away from the margin—where the Hadar Formation was deposited—toward the center of the Main Ethiopian Rift. This was associated with a notable northward propagation of volcanism since 3 Ma from the Ethiopian Rift into the Afar Depression (Lahitte et al., 2003).

Hadar Basin Stratigraphy

Major sedimentary accumulation began in the late Miocene to early Pliocene with fluviolacustrine deposits of the Sagantole Formation, which are correlated to the Middle Awash region further south and have been dated from 5.6 Ma to 3.9 Ma (Renne et al., 1999; Quade et al., 2004). The focus of this study is the Hadar Formation, which is composed of fluvial, paludal, and lacustrine deposits that rapidly accumulated (30–90 cm/k.y.) between ca. 3.8 and 2.9 Ma after normal faulting of the Sagantole Formation (Wynn et al., 2006). The Hadar Formation is defined (Taieb et al., 1976) and described in detail in the Hadar research area (Campisano, 2007; Campisano and Feibel, this volume). It is divided into four members separated by radiometrically dated tephras. The members, from bottom to top are: (1) the Basal Member, below the Sidi Hakoma Tuff (ca. 3.42 Ma), (2) the Sidi Hakoma Member, between the Sidi Hakoma Tuff and Triple Tuff-4 (ca. 3.25 Ma), (3) the Denen Dora Member, between Triple Tuff-4 and the Kada Hadar Tuff (ca. 3.20 Ma), and (4) the Kada Hadar Member, between the Kada Hadar Tuff and the Busidima unconformity surface (BUS; Wynn and Roman, this volume), which is located just above the Bouroukie Tuff 2

(BKT-2 ca. 2.95 Ma). Additional marker horizons are described in Campisano and Feibel (this volume). The Sidi Hakoma Member includes a lignite layer, gastropods beds, and the Kada Damum Basalt. The Denen Dora Member includes a widespread fluvial sandstone (DD-3 sand) below the Kada Hadar Tuff. The middle and upper parts of the Kada Hadar Member comprise the laminated "Confetti Clay," with the Kada Hadar Tuff a few meters below, and the BKT-1 and BKT-2 tuffs. Dating and correlation to the Hadar Formation are also provided by magnetostratigraphy in the Gona research area (Quade et al., this volume) and the Hadar research area (Aronson et al., 1977; Schmitt and Nairn, 1984; Renne et al., 1993; Tamrat et al., 1996). The accurate stratigraphic positions of reversals from the Hadar studies have been recently synthesized (Campisano, 2007). The Hadar Formation at Hadar falls within the Gauss normal-polarity chron 2An (C2An) and includes the reversed-polarity Kaena chron 2An.1r (C2An.1r) and Mammoth chron 2An.2r (C2An.2r), providing four additional correlation points at the well-dated boundaries of these chrons. The Hadar Formation is separated from the overlying Busidima Formation (ca. 2.7 to <0.6 Ma) by a major area wide, ~200 k.y. angular unconformity (Quade et al., this volume; Wynn et al., this volume). Below this unconformity, there are fluviolacustrine deposits; above it, there are conglomeratic fluvial channel deposits interpreted either as the ancestral Awash River (Quade et al., 2004; Wynn et al., 2006) or as alluvial fans from the Ethiopian Plateau (Yemane, 1997).

Paleoenvironments of the Hadar Formation

The regional and local tectonic context of deposition during Hadar Formation time is still poorly understood. The present location of the Hadar basin exposure at the margin of the Main Ethiopian Rift suggests a simple east-west extensional configuration with subsidence controlled by syndepositional down-drop along normal faults parallel to the Ethiopian escarpment such as the east-dipping As Duma fault (Quade et al., 2004). This is substantiated by records of eastward to northward paleodrainages (Tiercelin, 1986; Quade et al., 2004; Behrensmeyer, this volume). However, the Hadar Formation thickness increases eastward (Tiercelin, 1986; Walter, 1994) to northeastward (Wynn et al., 2006), conspicuously suggesting an increasing rate of subsidence toward the eastern rather than the western margin of the basin. As a result, it was recently suggested that the Hadar Formation was deposited in response to northeast-southwest extension associated with the Red Sea Rift system, and then it shifted to east-west extension associated with the Ethiopian Rift during deposition of the Busidima Formation (Wynn et al., 2006).

Paleoenvironmental studies generally show that during deposition of the Hadar and Busidima Formations, global cooling was associated with more arid conditions in Africa, with some environmental variability at various localities (Quade et al., 2004). Analysis of the Hadar faunal assemblage indicates a range of available habitats including open and closed woodlands, gallery forests, edaphic grasslands, and shrublands. The paleontological record indicates slightly more xeric conditions beginning around 3.2 Ma and a distinct faunal turnover at ca. 3.0 Ma, with evidence of an influx of more arid-adapted taxa (Campisano and Reed, 2007; Reed, 2008). Stable carbon isotope values from pedogenic carbonates at Gona indicate a gradual shift from woodlands to grassy woodlands in the early Pliocene, to more open, but still mixed, environments in the late Pleistocene, possibly associated with increasing aridity and fluctuations in the timing and source of rainfall (Levin et al., 2004). Pollen assemblages suggest a large biome shift, up to 5 °C cooling, and a 200 to 300 mm/yr rainfall increase just before 3.3 Ma, consistent with a global marine $\delta^{18}O$ isotopic shift (M2) (Bonnefille et al., 2004). Relative to modern East African lakes, $\delta^{18}O$ values from lacustrine mollusk shell horizons of the Hadar Formation indicate large and high-frequency lake-level fluctuations that point to wetter and probably cooler summers, possibly attributable to the strengthening of the Atlantic-derived air mass component to the Ethiopian monsoon (Hailemichael et al., 2002). However, the timing and periodicity of the climate variations observed in these studies are still insufficiently precise to allow definite correlation to known regional and global climate conditions accurately constrained in the marine realm.

CHRONOSTRATIGRAPHIC ANALYSIS

Stratigraphic and Geochemical Correlations

Compared to Hadar and Gona, the Hadar Formation deposits in the Ledi-Geraru area are generally thicker and more distal from the source region, and there is a predominance of lacustrine over fluvial deposits. Therefore, they provide better preservation and resolution of the paleoenvironmental history. The stratigraphy is best exposed at the Middle Ledi section (Fig. 1) where sediments are relatively uninterrupted by faulting and essentially flat lying, with a low bedding dip of 0°–2° (<5°) to north-northwest. As a result, the stratigraphy is exposed along a south-to-north transect of several kilometers on strata well-exposed on small hills and along ridges. The Middle Ledi section is a composite of ten overlapping subsections correlated to each other using unambiguous marker beds. The composite section spans an ~230-m-thick continuous sedimentary interval including the complete Sidi Hakoma and Denen Dora Members (Fig. 2). The Sidi Hakoma Tuff, Triple Tuff-4, and the Kada Hadar Tuff are correlated between the Hadar and Ledi-Geraru research areas using the following stratigraphic relationships and lithologic descriptions.

Sidi Hakoma Tuff (SHT)

The Sidi Hakoma Tuff is typically preserved in the region as a widespread white bentonite, ~20 cm thick, overlying Basal Member fluvial-deltaic sands. Exposures immediately west and south of the Middle Ledi section are located a few meters above the level of the modern Awash floodplain along the course of the river. Vitric channel-fill and crevasse-splay deposits of the Sidi Hakoma Tuff are also preserved at both Hadar and Dikika (Wynn

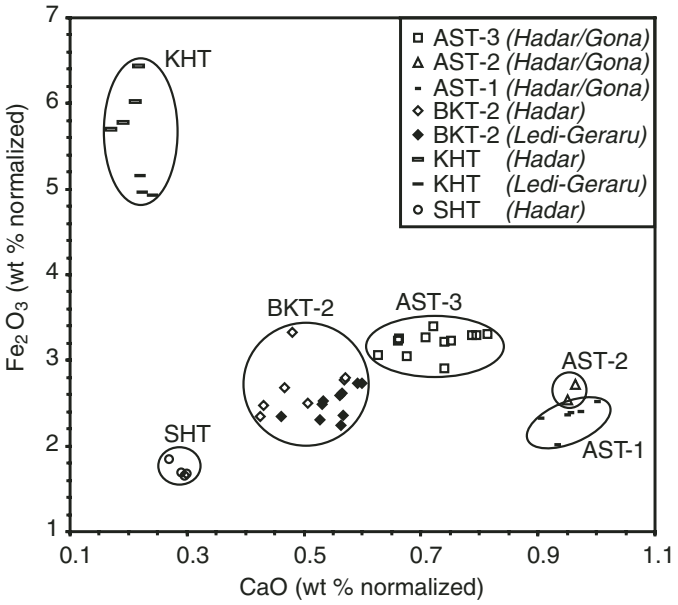

Figure 2. Normalized bivariate plot showing major-element composition from various tuffaceous horizons from the Hadar, Gona, and Ledi-Geraru research areas. Hadar/Gona data are from Hart et al. (1992) and Campisano (2007). Ledi-Geraru data are from DiMaggio et al. (this volume).

et al., 2006; Campisano and Feibel, this volume). A 25-cm-thick white bentonite located near the bottom of the Middle Ledi section (~4.15 m level) matches the description of the Sidi Hakoma Tuff bentonite exposed to the west and south. It is found above sands presumably of the Basal Member. The lack of a vitric facies in the Middle Ledi section precludes a definitive geochemical correlation to the Sidi Hakoma Tuff, but the tuff's lithology, position on the Awash floodplain, and associated context provide suitable evidence for a correlation. A unique lignite layer associated with a thin (~2 cm) white bentonite and a *Corbicula* shell horizon at approximately the 40 m level provides additional evidence that the basal bentonite represents the Sidi Hakoma Tuff. A similar lignite layer is known from the middle of the Sidi Hakoma Member in both central Hadar and along the border of the Hadar and Ledi-Geraru research areas (at Hurda wadi; Tiercelin, 1986). Furthermore, the lignite layer in central Hadar is also associated with thin bentonites and a *Corbicula* shell horizon, referred to as the Kada Me'e Tuff Complex (Campisano and Feibel, this volume).

Triple Tuff 4 (TT-4)

Although none of the Triple Tuffs preserves a vitric component, their unique lithologic context (specifically that of Triple Tuff-4), is diagnostic. At Hadar and Dikika, Triple Tuff-4 is a ubiquitous white bentonite encased in an olive-green laminated fissile-shale that preserves apatite nodules and an ostracodite unit in its lower portion (Tiercelin, 1986; Wynn et al., 2006). In the Middle Ledi section, a similar lithologic unit at the 151 m level (150.87 ± 0.675 m) is proposed as a correlate to the Triple Tuff-4/ostracod-shale unit. This laminated olive-green shale preserves a white bentonite, apatite nodules, and low concentrations of ostracods. Instead, the lower half of the shale contains a high concentration of *Melanoides* shells and carbonized plant pieces. However, *Melanoides* shells are occasionally preserved below the ostracodite at Hadar, and ostracod abundance was observed to be significantly lower in the Hurda Wadi Triple Tuff-4 exposures compared to central and western Hadar (Campisano, 2007, personal commun.). Based on its lithologic and interpreted chronostratigraphic position (see following), we propose this sequence as a correlate to the Triple Tuff-4/ostracod-shale from Hadar.

Kada Hadar Tuff (KHT)

At Hadar, the Kada Hadar Tuff is typically preserved as a beige, silty bentonite, 20–80-cm thick, but vitric channel-fill deposits (likely crevasse-splay channels) are occasionally preserved (Yemane, 1997; Campisano, 2007). A 1–2-m-thick vitric channel fill preserved at the top of the Middle Ledi section is similar in outcrop appearance to the Hadar Kada Hadar Tuff channel-fill deposit. This tephra deposit is not laterally continuous in the uppermost part of the section, and it is separated from better-exposed underlying strata by colluvial cover. Its stratigraphic position has been measured both by direct thickness measurements (yielding 228.34 m level) and by derivation from measured horizontal distances assuming constant dip from an exposed underlying outcrop (yielding 227.53 m level). A conservative 2 m uncertainty allowing for dip variations was thus attributed to the direct thickness measurements, yielding a 229.34 ± 3.00 m level within the 2-m-thick tuff. The BKT-2 complex was positively identified (DiMaggio et al., this volume) well above the proposed Kada Hadar Tuff correlate (perhaps by as much as 60–100 m, although the exact stratigraphic distance was not determined), confirming that the Ledi-Geraru research area includes almost the entire Hadar Formation, from at least Sidi Hakoma Tuff to BKT-2. The Kada Hadar Tuff correlation is confirmed by diagnostic major-element glass chemistry (Fig. 2; Table 1). Glass from the Kada Hadar Tuff is chemically distinct from all other Hadar Formation tephra in its exceptionally low concentrations of Al_2O_3 and CaO and high concentrations of Fe_2O_3. When compared to existing geochemical data from other vitric tephra horizons from the Hadar Formation (Hart et al., 1992; Walter, 1994; Campisano, 2007; DiMaggio et al., this volume), the Middle Ledi Kada Hadar Tuff is clearly distinct from the Sidi Hakoma Tuff and BKT-2 of the Hadar Formation as well as the AST series of tephra of the Busidima Formation (Table 1). The Middle Ledi sample displays the low Al_2O_3 and CaO and high Fe_2O_3 concentrations diagnostic of the Kada Hadar Tuff and is within 1σ uncertainty for virtually all major elements. The slightly larger spread in Fe_2O_3 values is within the expected error related to minor differences in analytical procedure. Based on these congruent analyses, we conclude that the vitric tuff horizon located at the top of the Middle Ledi stratigraphic section is confidently identified as the Kada Hadar Tuff.

TABLE 1. MAJOR-ELEMENT GEOCHEMISTRY OF THE KADA HADAR TUFF

Sample	*n*		SiO_2	TiO_2	Al_2O_3	MnO	Fe_2O_3	MgO	CaO	Na_2O	K_2O	Total
Middle Ledi												
AM06-1047	21	avg	73.96	0.27	9.69	0.18	4.51	0.05	0.21	0.92	1.16	90.95
		±1σ	1.03	0.04	0.21	0.05	0.29	0.07	0.02	0.17	0.16	1.20
AM06-1047	8	avg	72.54	0.30	9.89	0.15	4.61	0.01	0.20	0.89	0.90	89.50
		±1σ	0.63	0.05	0.32	0.08	0.16	0.02	0.03	0.48	0.30	1.14
AM06-1047	5	avg	74.08	0.28	9.69	0.15	4.48	0.03	0.22	0.90	1.27	91.09
		±1σ	0.24	0.03	0.18	0.03	0.25	0.04	0.02	0.36	0.31	0.39
Hadar												
E02-7413.AV	15	avg	70.55	0.26	8.98	0.20	5.40	0.02	0.19	2.40	1.57	89.76
		±1σ	2.41	0.04	0.33	0.04	0.37	0.01	0.03	0.49	0.20	3.04
E01-7341.AV	14	avg	69.21	0.27	8.78	0.19	5.63	0.01	0.19	1.61	1.38	87.49
		±1σ	1.66	0.03	0.16	0.06	0.31	0.01	0.03	0.39	0.15	1.49

Note: Samples were analyzed by electron microprobe; *n*—number of analysis; avg—average values listed as wt% with associated standard deviation (1σ).

Paleomagnetic Sampling

The Middle Ledi section was measured to within centimetric precision for 200.24 m total thickness starting 4.15 m below the base of the Sidi Hakoma Tuff. In the last 30-m-thick section below the Kada Hadar Tuff, sampling and logging were hindered by the poor exposure. Sampling of 2.5-cm-diameter cylindrical rock cores was performed with an electric drill mounted with a diamond-coated bit and cooled with an electric air compressor, both devices powered by a portable generator. Cores were oriented with a compass corrected for local declination (1.7°). One core was sampled at each of the 401 stratigraphic levels separated by an average interval of ~50 cm. All encountered lithologies were sampled. Meter-thick lenticular sandstone beds were avoided as much as was allowed by the outcrop configuration to avoid possible hiatuses associated with the erosional scouring typical of these high-energy deposits. Corrections of negligible bedding tilts were not applied due to the low magnitude of measured dips (<5°) and the potential error associated with the measurements of such low dips.

Paleomagnetic Analysis

Demagnetization and Characteristic Remanent Magnetization (ChRM)

Remanent magnetizations of samples were measured on a 2G Enterprises DC SQUID cryogenic magnetometer. Thermal demagnetization was performed at up to 18 thermal steps in a shielded furnace at the Utrecht University paleomagnetic laboratory. A first selection of pilot samples distributed every 4 m throughout the sampled stratigraphy was stepwise thermally demagnetized in great detail in order to determine characteristic demagnetization behavior, establish the most efficient demagnetization temperature steps, and localize stratigraphic intervals with potential paleomagnetic reversals. These results guided further processing of a second selection of samples at higher stratigraphic resolution from key parts of the section. This ultimately enabled us to distinguish between reliable and less reliable results and to confidently locate reversals in the stratigraphy. In total, 236 samples were thermally demagnetized.

Two main characteristic remanent magnetization (ChRM) components stand out clearly on vector end-point diagrams and stereographic projections. A low-temperature component (LTC) with only normal-polarity directions is typically demagnetized from ~100 °C to 250 °C. A high-temperature component (HTC) with normal- or reversed-polarity directions decays from ~350 °C to 525 °C (Fig. 3A). On average, 60% of the LTC remanence was quickly removed by 250 °C, leaving a slow decaying HTC up to 525 °C. Generally the remanence reached near-zero values above 550 °C, but in some samples, a higher-temperature component concordant with the HTC was recorded from 550 °C to >620 °C. In some of these samples, the contribution of the LTC was indicated by a normal direction overlapping on a reversed-polarity direction carried by the HTC (Fig. 3B). The LTC was found exclusively with a normal-polarity orientation, while HTC show normal and reverse polarity. This clearly identifies the LTC as a normal overprint. In a majority of samples, the HTC is well expressed, enabling straightforward isolation of normal- or reversed-polarity directions. However, in some samples, the HTC was poorly preserved and did not yield reliable directions (Fig. 3B). For these, overlapping LTC, although usually removed below 350 °C, could be found, extending in a few cases as high as 450 °C, thus indicating the maximum extent of the LTC contribution. This information was crucial for selecting reliable normal-polarity direction. All normal-polarity directions that did not extend beyond 450 °C were considered to be a possible overprint and thus unreliable for further analysis (Fig. 3C).

Rock Magnetism and Magnetic Mineralogy

Rock magnetic experiments were performed to assess the magnetic mineralogy and to better constrain the reliability of the ChRM. To test for potential artifacts due to mineral transformation during stepwise heating, alternating field (AF) demagnetization was performed on 29 pilot samples (Fig. 3D). These AF results show the same general behavior as the thermal demagnetization. This indicates that mineral transformation upon heating

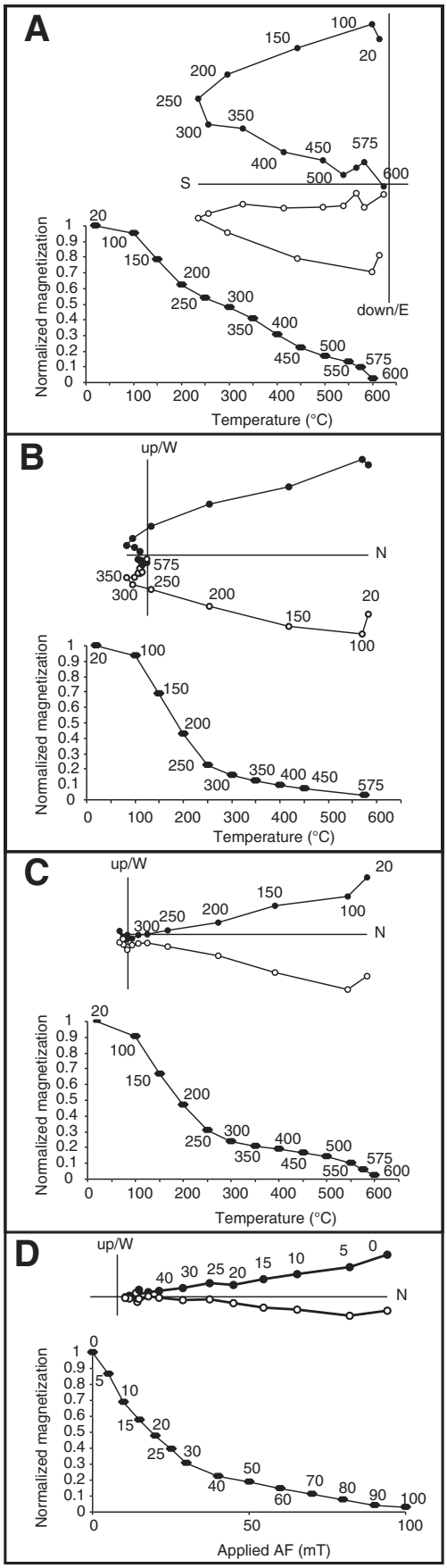

Figure 3. Typical demagnetization behaviors. Top diagrams: vector end point of typical thermal (A, B, C) or alternating field (AF) (D) demagnetizations. Full (open) symbols are projections on horizontal (vertical) plane. Bottom diagrams: normalized magnetization versus temperature or applied field. (A) Typical thermal demagnetization (quality 1). (B) Strong normal overprint (quality 3). (C) Full normal overprint (rejected). (D) Typical AF demagnetization.

did not significantly alter the results. However, AF treatment was less effective in separating the ChRM components.

High-temperature-range thermomagnetic experiments were performed on dry bulk sediments from five representative samples of various lithologies of the investigated stratigraphic section. Measurements using the KLY3-CS bridge show that (1) during heating, a slight susceptibility increase between room temperature and 300–400 °C is followed by a nearly linear decrease up to ~550 °C and a main drop between 550 and 580 °C; and (2) during cooling, susceptibility curve is irreversible below 500 °C (Fig. 4A, lower panel). This irreversibility at lower temperatures suggests the initial presence of maghemite or titanomaghemite altered during heating and therefore not apparent during cooling. The main drop between 550 and 580 °C is characteristic of fine-grained magnetite or Ti-poor titanomagnetite. These results are consistent with high-field thermomagnetic runs performed on a Curie balance, which also show a quasi-linear decrease during ~350–500 °C heating with a slightly sharper moment decrease above 500 °C and an irreversible cooling curve (Fig. 4A, upper panel). These thermomagnetic results, along with the thermal and AF demagnetization behavior and typically high values of NRM and susceptibility (Table DR1[1]), rule out iron sulfides, goethite, or hematite as important contributors to the remanence. However, the results strongly suggest the predominance of fine-grained magnetite and/or Ti-poor titanomagnetite for the HTC, as well as the influence of maghemite and/or titanomaghemite on the LTC.

Low-temperature-range thermomagnetic experiments were performed on dry bulk sediments from five other representative samples using a Quantum Design Magnetic Properties Measurement System (MPMS) at the Faculty of Geosciences at the University of Bremen (Fig. 4B). All zero-field-cooled and field-cooled curves (temperature range 5–300 K, applied field 5 T) lack the indication of stoichiometric magnetite usually shown by the Verwey structural phase transition at ~120 K (Franke et al., 2007). The shift to a lower-temperature transition would be indicative of (1) nonstoichiometric, slightly oxidized magnetite (the Verwey transition can be totally suppressed at a sufficiently high degree of maghematization) or (2) sufficiently high Ti-rich magnetite (the Verwey transition can be totally suppressed at Ti contents > 0.04; Kakol et al., 1994). The presence of Ti-bearing magnetic mineral phases in the samples is further supported by the characteristics of the curves of the low-temperature thermomagnetic

[1]GSA Data Repository item 2008194, which includes tabulated characteristic remanent magnetization directions, is available at www.geosociety.org/pubs/ft2008.htm, or on request from editing@geosociety.org, Documents Secretary, GSA, P.O. Box 9140, Boulder, CO 80301-9140, USA.

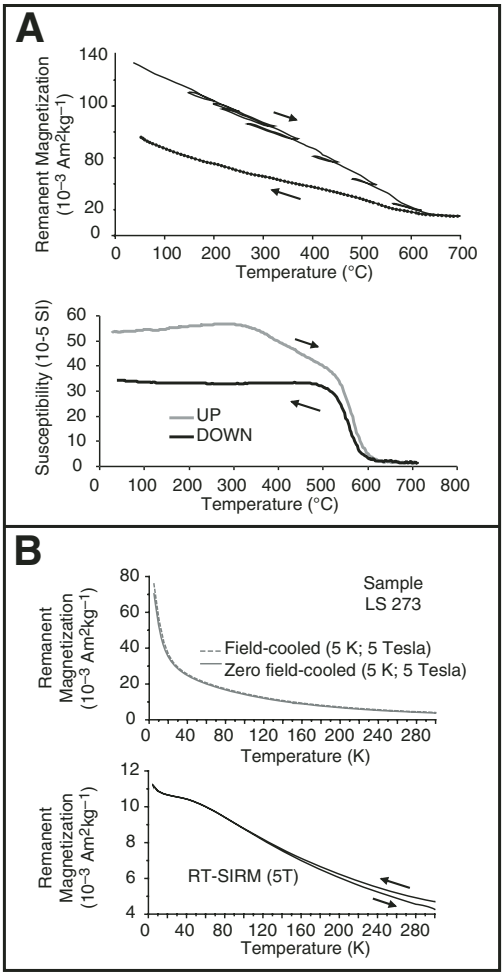

Figure 4. (A) Thermomagnetic experiments. Top diagram: typical high-field magnetic moment upon heating and subsequent cooling in successive temperature ranges measured on Curie balance. Bottom diagram: typical low-field susceptibility upon heating and subsequent cooling measured on kappabridge KLY3-CS. (B) Low-temperature Magnetic Properties Measurement System (MPMS). Top diagram: zero-field-cooled (solid line) and field-cooled (dotted line) remanence (5 T applied field) monitored between 5 and 300 K. Bottom diagram: Low-temperature cycle (between 300 and 5 K) of the room-temperature saturation isothermal remanent magnetization (RT-SIRM, 5 T). Black arrows mark the cooling and subsequent warming curve.

runs (cycled between 300 and 5 K, 5 T applied field at room temperature; RT-SIRM, Fig. 4B, lower panel), which indicate a mixed signal of Ti-poor titanomagnetites and Ti-rich titanohematites (Dillon and Franke, 2008) since the presence of notable amounts of pure hematite or goethite has already been excluded. This characteristic mineral combination supports a basaltic origin as the main source of the magnetic material (e.g., Dunlop and Özdemir, 1997; Krása et al., 2005). Parallel conclusions have been reached by Tamrat et al. (1996) based on extensive rock magnetic experiments on samples from comparable lithologies collected from the Hadar research area. They show similar thermomagnetic curves and thermal demagnetization behavior. In addition, they provide hysteresis measurements and three-component IRM experiments showing a dominant low-coercivity component demagnetized below 600 °C. These further suggest a remanence dominated by pseudo–single-domain titanomagnetite clearly associated with the HTC, and a minor contribution from a higher-coercivity mineral such as titanomaghemite.

To further test these suggestions, scanning electron microscopic (SEM) analyses were performed on polished sections of the five representative samples also used for the MPMS measurements described above, using a FEI XL30 SFEG SEM at the Utrecht Electron Microscopy facility at 15 kV acceleration voltage. A thin carbon coating of a few nanometers was applied on the polished sections to avoid surface charging. Backscattered electron imaging was used for visualizations, and energy-dispersive X-ray spectroscopy was used to examine the elemental composition. Recorded elemental spectra were normalized to their respective oxygen maxima. EDAX PhiRhoZ processing software was used to (semi-) quantify the obtained elemental spectra. The micrographs and element spectra show detrital grains of iron (-titanium) mineral phases within the spatial resolution of the SEM within a 0.1–100 µm grain-size range (Fig. 5). Element spectra show magnetite composition (Fig. 5A, 1) and Fe:Ti ratios indicative of (Ti-rich) titanohematites ($Fe_{3-x}Ti_xO_4$, $0 \le x \le 1$) (Fig. 5B, 1, 3, and 5) and Ti-poor titanomagnetites ($Fe_{2-y}Ti_yO_3$, $0 \le y \le 1$)) (Fig. 5B, 2, 4, and 6), which were calculated according to their stoichiometric formulas (Table 2). The magnetic grains contain minor amounts of metal ions other than Fe and Ti, because substitution of Fe by Mg or Al is a typical phenomenon in detrital (titano-) magnetite. To account for this effect, the total of these three elements (Fe_Σ) was calculated according to Dillon and Franke (2008). The calculated titanomagnetite compositions therefore range between TM09 and TM54, while the titanohematite grains have compositions close to pure ilmenite (TH89 to TH98). According to Buddington and Lindsley (1964), the ilmenite content in a titanohematite phase coexists with a titanomagnetite phase of complementary composition. This intergrowth would be typical for low-temperature exsolution processes of slow-cooling basaltic rocks. The resulting domain size of the titanomagnetite is therefore expected to be much smaller than the observed overall particle sizes because it is restricted by the lamellae formed by the titanohematite. The detrital character of these (titano-) magnetites and titanohematites is evident by their fragmental appearance, relatively smooth surfaces, and sharp, curved edges related to shrinkage cracks (Fig. 5B). These indicate variable degrees of maghematization of the grains and thus further support the detrital basaltic origin of the magnetic mineralogy.

Basaltic grains were most probably derived from the numerous basaltic flows available in the drainage basin of the Afar Rift. Recent weathering of these titanomagnetites during the Brunhes normal interval may have produced a chemical remanent magnetization in the titanomaghemite that overprinted, sometimes completely, the original detrital remanent magnetization.

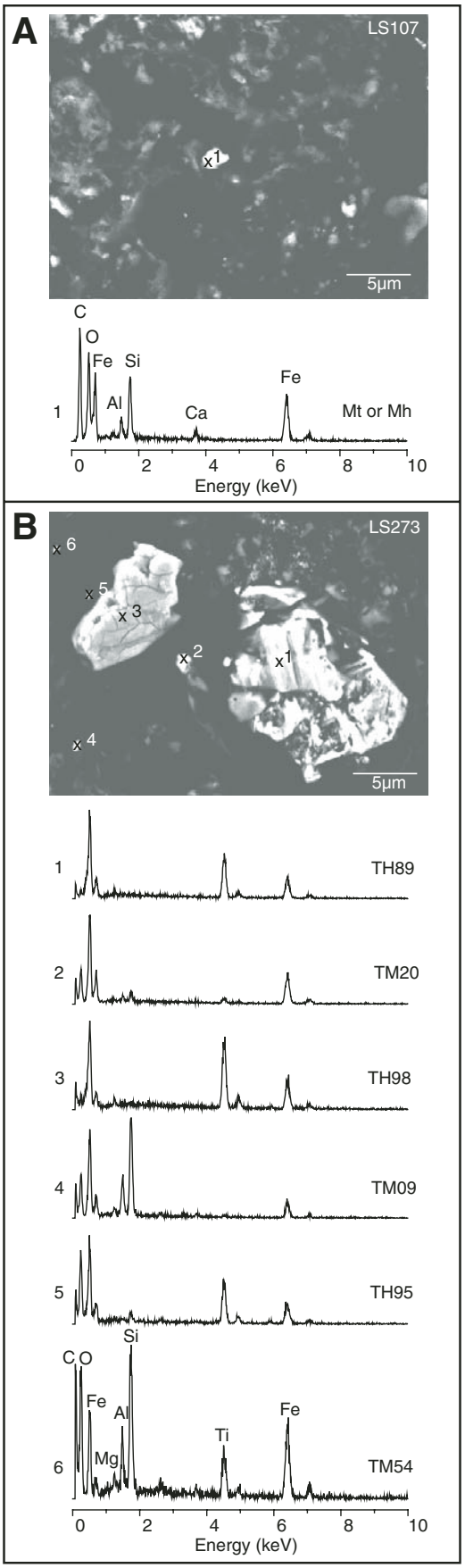

Figure 5. Backscatter electron micrographs and associated energy-dispersive X-ray spectra from spot analyses marked by cross symbols in samples (A) LS107 and (B) LS273. Whiteish particles correspond to opaque minerals, rich in Fe and Ti (Mh—maghemite, Mt—magnetite, TH—titanohematite, TM—titanomagnetite).

ChRM Direction Analysis

ChRM directions were calculated using least square analysis (Kirschvink, 1980) on a minimum of four consecutive steps of the HTC. Line fits were not anchored to the origin. ChRM directions with maximum angular deviation (MAD) above 30° were systematically rejected. Careful selection of ChRM directions (especially of normal polarity directions) is required by the recognized occurrences of a normal overprint potentially extending to relatively high demagnetization temperatures (450 °C). For 93 samples, normal- and reversed-polarity directions were clearly identified on the HTC, where linear decay extended several temperature steps above 450 °C (quality-1 directions, Table DR1 [see footnote 1]). For 69 samples, normal or reversed polarities are indicated but are less reliable (quality-2 directions) because of directional scatter and/or LTC overlap on HTC, resulting in directions slightly divergent from ideal univectorial decay toward the origin. For 57 unreliable samples (quality-3 directions), normal- or reverse-polarity determination is ambiguous due to a strong normal-polarity LTC extending up to 450 °C that partially or fully overprints the HTC. For these samples, unambiguous polarity determination was virtually impossible, especially for HTC of normal polarity. However, for some HTC of reversed-polarity direction, a ChRM direction could be calculated through line fit forced to the origin or through great circle analysis (using the mean of quality-1 reversed directions as set reference point according to the methods of McFadden and McElhinny, 1988), and these were graded as quality-3. To avoid misinterpreting normal overprints as primary record of the magnetic field, which would ultimately result in constructing an erroneous magnetostratigraphic record, we opted for the conservative approach and rejected quality-2 and quality-3 directions altogether from the following magnetostratigraphic record. The remaining set of 93 quality-1 ChRM directions cluster around

TABLE 2. CATION ELEMENTAL CONTENTS

Sample	Particle	Ti (%)	Fe_{Σ} (%)	Fe_{Σ}/Ti	Mineral
LS273	1	14.36	17.93	1.25	TH89
LS273	2	1.12	15.82	14.13	TM20
LS273	3	18.5	19.37	1.05	TH98
LS273	4	0.3	9.69	32.30	TM9
LS273	5	7.07	7.84	1.11	TH95
LS273	6	3.28	14.8	4.51	TM54
LS107	1	0	11.14	—	Mt or Mh

Note: Particle—Label of particle on Figure 5; Ti—element atomic % from semiquantitative energy-dispersive spectroscopy (Fig. 5); Fe_{Σ}—sum of Fe, Al, and Mg element atomic %; Mineral—mineral phase calculated according to Dillon and Franke (2008); TM—titanomagnetite; TH—titanohematite; Mt—magnetite; Mh—maghemite.

antipodal normal- and reverse-polarity mean directions (Fig. 6A) and pass the reversals test, suggesting that our selection procedure was successful in excluding directions biased by the normal overprint (Tauxe, 1998).

Virtual geomagnetic poles (VGP) were calculated from the remaining quality-1 directions, and the Vandamme (1994) criterion was applied to the VGPs. Eleven widely outlying VGPs were excluded by the Vandamme procedure and downgraded to quality-2 directions. The resulting set of 82 quality-1 ChRM directions provides reliable paleomagnetic polarity at an average interval of 2.4 m throughout the sampled section.

Rotation and Flattening of Paleomagnetic Directions

To compare our results to expected paleomagnetic poles, we computed the mean direction using quality-1 ChRM directions with MAD below 15° only (74 directions). The mean of combined normal and reverse directions was compared to the expected direction from the geocentric axial dipole (GAD) or to the expected direction calculated from the apparent polar wander path (APWP) of stable Africa (computed from 25 African poles with mean ages of 3.1 Ma; Besse and Courtillot, 2002). In both cases, results show, at 95% confidence level, that the mean inclination is significantly too shallow by ~5°–10°, while the mean declination is significantly rotated by ~5°–10° in a counterclockwise sense (Table 3). These values can be considered as minimum estimates because bedding tilt correction of the observed low-magnitude dips (0°–5° in northerly direction) was not performed on these data and would increase rotation and flattening by 0°–5°. Our results compare well with previously reported paleomagnetic directions from the same age at the Hadar section (Tamrat et al., 1996), which also show significant flattening and ~5° counterclockwise rotation when compared to the APWP of Africa (although rotation is statistically insignificant if compared to the GAD).

Paleomagnetic results suggest that a small counterclockwise rotation (~5°–10°) has affected the region after deposition of these rocks since ca. 3 Ma. This may reflect subsequent deformation of the Hadar Basin, possibly associated with the extension of the Afar Rift during the 3–1 Ma northward propagation of Stratoid Series volcanism (Manighetti et al., 2001; Lahitte et al., 2003; Wolfenden et al., 2004). Similar to Tamrat et al. (1996), we observe ~5°–10° flattening of inclination interpreted to result from sedimentary processes during deposition and compaction. This is supported by successful correction of flattening using the method of Tauxe (2005). The observed shallow inclination of 11.5° ± 4.9° is corrected to 21.3° (95% confidence interval is 17–26°; Fig. 6B). This compares well with the expected inclination (16.4° ± 4.9° for the APWP or 21.5° for the GAD). In addition to the reliability tests and quality selection of the ChRM directions, the rotation and successful correction of flattening further support a primary and detrital origin of the remanent magnetization. Thus, the selected directions are suitable for constructing a reliable magnetostratigraphic section.

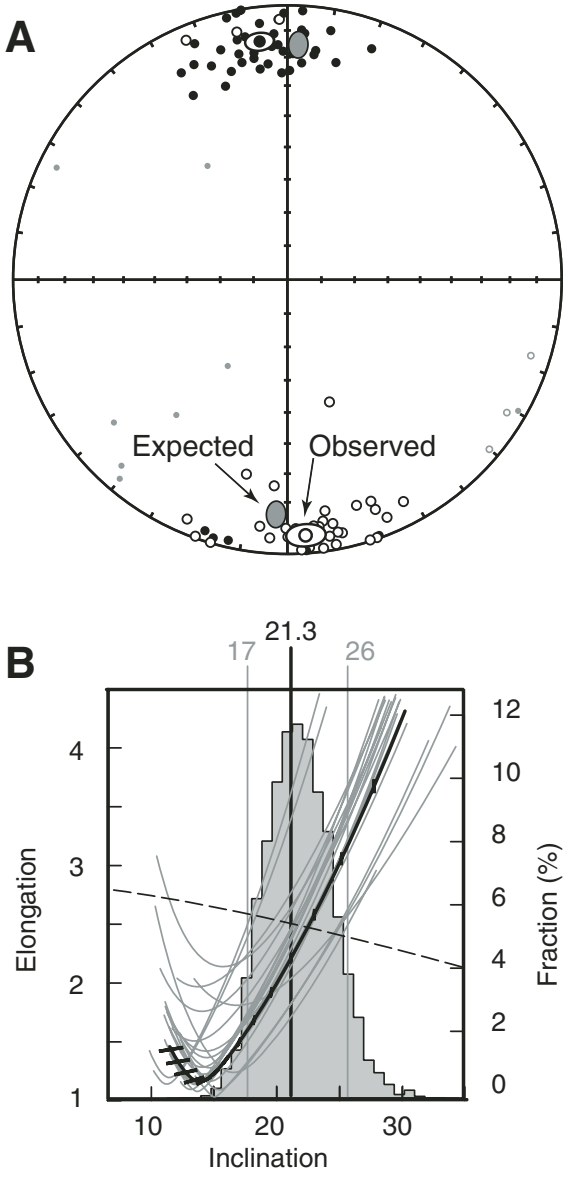

Figure 6. (A) Characteristic remanent magnetization (ChRM) directions projected in lower (full symbol) and upper (open symbol) hemispheres of stereogram. Smaller symbols are 11 directions rejected by Vandamme (1994) criterion. The observed means of normal and of reversed ChRM directions are compared to the expected direction calculated from the apparent polar wander path (APWP) of Africa at 3.1 Ma (Besse and Courtillot, 2002) at the site location (Table 3). The flattened distribution of the ChRM directions contrasts with the north-south–elongated distribution expected for geomagnetic directions at these low latitudes. (B) Correction of observed (Obs.) inclination error using the method developed in Tauxe (2005) applied to the quality-1 ChRM directions with maximum angular deviation (MAD) < 15° (n = 72). Black curve shows variation of the elongation of the data set distribution with respect to mean inclination when affected by a flattening factor ranging from 0.35 to 1.00; light-gray curves are the same for generated data sets from bootstrap analysis. The corrected inclination is given by the intersection with the expected elongation (dotted curve) from the geomagnetic model. Background histograms indicate distribution of corrected inclinations with mean of 21.3° and 95% confidence interval (17°–26°).

TABLE 3. MEAN PALEOMAGNETIC DIRECTIONS

Data set	Observed mean direction					Rotation	Flattening	Reference pole				Expected I	Expected D
	D_s (°)	I_s (°)	α_{95} (°)	k	n	R ± ΔR (°)	F ± ΔF (°)	Age	Lat. (°N)	Long. (°E)	A_{95} (°)	I_x ± δI (°)	D_x ± δD (°)
Middle Ledi (this study)													
Q-1	354.4	11.4	2.9	30.5	82	–8.3 ± 3.2	5.0 ± 4.5	3.1	86.2	176.9	2.6	16.4 ± 4.9	2.7 ± 2.6
Q-1	354.4	11.4	2.9	30.5	82	–5.6 ± 2.4	10.1 ± 2.3	GAD	90	180.0	0	21.5 ± 0.0	0.0 ± 0.0
Q-1 MAD<15	354.8	11.5	3.1	29.4	74	–7.9 ± 3.3	4.9 ± 4.6	3.1	86.2	176.9	2.6	16.4 ± 4.9	2.7 ± 2.6
Q-1 MAD<15	354.4	11.5	3.1	29.4	74	–5.6 ± 2.5	10.0 ± 2.5	GAD	90	180.0	0	21.5 ± 0.0	0.0 ± 0.0
Hadar (Tamrat et al., 1996)													
Tamrat, 1996	358.6	7.0	4.0	17.9	72	–4.1 ± 3.8	9.4 ± 5.1	3.1	86.2	176.9	2.6	16.4 ± 4.9	2.7 ± 2.6
Tamrat, 1996	358.6	7.0	4.0	17.9	72	–1.4 ± 3.2	14.5 ± 3.2	GAD	90	180.0	0	21.5 ± 0.0	0.0 ± 0.0

Note: Data set—averaged paleomagnetic data set of ChRM directions (Q-1 indicates mean of quality-1 ChRM directions; Q-1 MAD < 15 indicates mean of quality-1 ChRM directions with maximum angular deviation [MAD] less than 15°; Tamrat et al., 1996). ChRM directions are from Tamrat et al. (1996). Observed mean directions: D_s—mean declination; I_s—mean inclination; α_{95}—angular radius of 95% confidence; k—concentration parameter; n—number of averaged ChRM directions. Rotation R ± ΔR (Flattening F ± ΔF)—difference and 95% confidence between the observed mean declination (inclination) and the declination (inclination) expected from the apparent polar wander path (APWP) of Africa at 3.1 Ma (Besse and Courtillot, 2002) at the site location (11.13°N, 40.67°E).

Magnetostratigraphic Analysis

Correlation to the Paleomagnetic Polarity Time Scale

Three distinct paleomagnetic polarity intervals separated by two reversals are clearly identified by the distribution of normal and reverse quality-1 directions (Fig. 7). The consistency of the polarity of quality-1 directions within those polarity intervals further supports the reliability of our data-selection procedure. At both reversals, careful demagnetization of all collected samples was performed to obtain the best possible resolution for the stratigraphic position of these reversals, resulting in positions of 99.05 ± 4.00 m for the bottom reversal and 191.11 ± 3.40 m for the top reversal. The thickness of these inversion intervals and the fewer quality-1 directions within them are consistent with the typical duration of weak transitional geomagnetic field during reversals (Clement et al., 2004; Valet et al., 2005).

Correlation to the paleomagnetic polarity time scale is indicated by the age of the tuff horizons recognized in the Middle Ledi sections and correlated to dated composite sections from the Hadar research area (Fig. 7). Similar to the pattern found in these other sections, the Sidi Hakoma Tuff and the Kada Hadar Tuff bracket a reversed interval that includes Triple Tuff-4 and is therefore unmistakably recognized as the Mammoth C2An.2r. The two identified reversals thus provide two age constraints to the Middle Ledi section in addition to the three dated tie points supplied by the correlation of the Sidi Hakoma Tuff, Triple Tuff-4, and the Kada Hadar Tuff.

Age References

To derive sediment accumulation rates from these five age reference tie points, we present below a review of the present level of precision and accuracy on these age estimates. The reference ages for the Mammoth C2An.2r boundaries have been revised since the last publications of magnetostratigraphic results from the Hadar Formation (Renne et al., 1993; Tamrat et al., 1996). These previous ages (3.330 Ma and 3.220 Ma for the bottom and top of the Mammoth C2An.2r, respectively) relied on the astronomically calibrated Pliocene time scale established by Hilgen (1991) based on the correlation of sedimentary cycles from Mediterranean marine successions to the precession time series of the astronomical solution of Berger and Loutre (1991). However, application of recent astronomical solutions (Laskar et al., 2004), which provide a better fit to the Mediterranean record, yields an updated time scale with 3.330 Ma and 3.207 Ma ages for the bottom and top of the Mammoth C2An.2r, respectively (Lourens et al., 1996, 2004). More recently, Lisiecki and Raymo (2005) revised these ages to 3.319 Ma and 3.210 Ma, respectively, based on a stack of 57 globally distributed benthic $\delta^{18}O$ records. Errors in these astronomical solutions may arise from uncertainties of tidal dissipation and changes in global ice volume altering Earth's dynamical ellipticity (Lourens et al., 2001), but the best fit to the Mediterranean record is obtained with present-day values of tidal dissipation and dynamical ellipticity, suggesting that these values have not significantly altered the Pliocene-Pleistocene record (Lourens et al., 1996). However, remaining uncertainties in the time lag among astronomical forcing, climate response, and registration in the stratigraphic record, and the assumption of a constant sedimentation rate between astronomically calibrated points, must be accounted for when constructing the time scale. Although these parameters are not readily resolvable, we apply a reasonable bracket for the related error previously proposed by Kuiper et al. (2004), by assigning a ±5 k.y. uncertainty to all the astronomically calibrated ages.

The ages of the three identified tuffaceous layers within the Middle Ledi section are provided by stratigraphic correlations to the Sidi Hakoma Tuff (SHT), Triple Tuff-4 (Triple Tuff-4), and the Kada Hadar Tuff (KHT), previously dated by $^{40}Ar/^{39}Ar$ at Hadar to 3.397 ± 0.029 Ma, 3.220 ± 0.012 Ma, and 3.175 ± 0.012 Ma, respectively; ages are given with their analytical error (Walter and Aronson, 1993; Walter, 1994). Since the publication of these ages, new intercalibration of the neutron fluence monitor standard (Fish Canyon Tuff sanidine age increased from 27.84 to 28.02 Ma by Renne et al., 1998) yields revised ages of 3.419 ± 0.029 Ma, 3.241 ± 0.012 Ma, and 3.196 ± 0.012 Ma for the Sidi Hakoma Tuff, Triple Tuff-4, and Kada Hadar Tuff, respectively. For the Sidi Hakoma Tuff, an independent age estimate of 3.41 ± 0.01 Ma is provided via geochemical correlation to

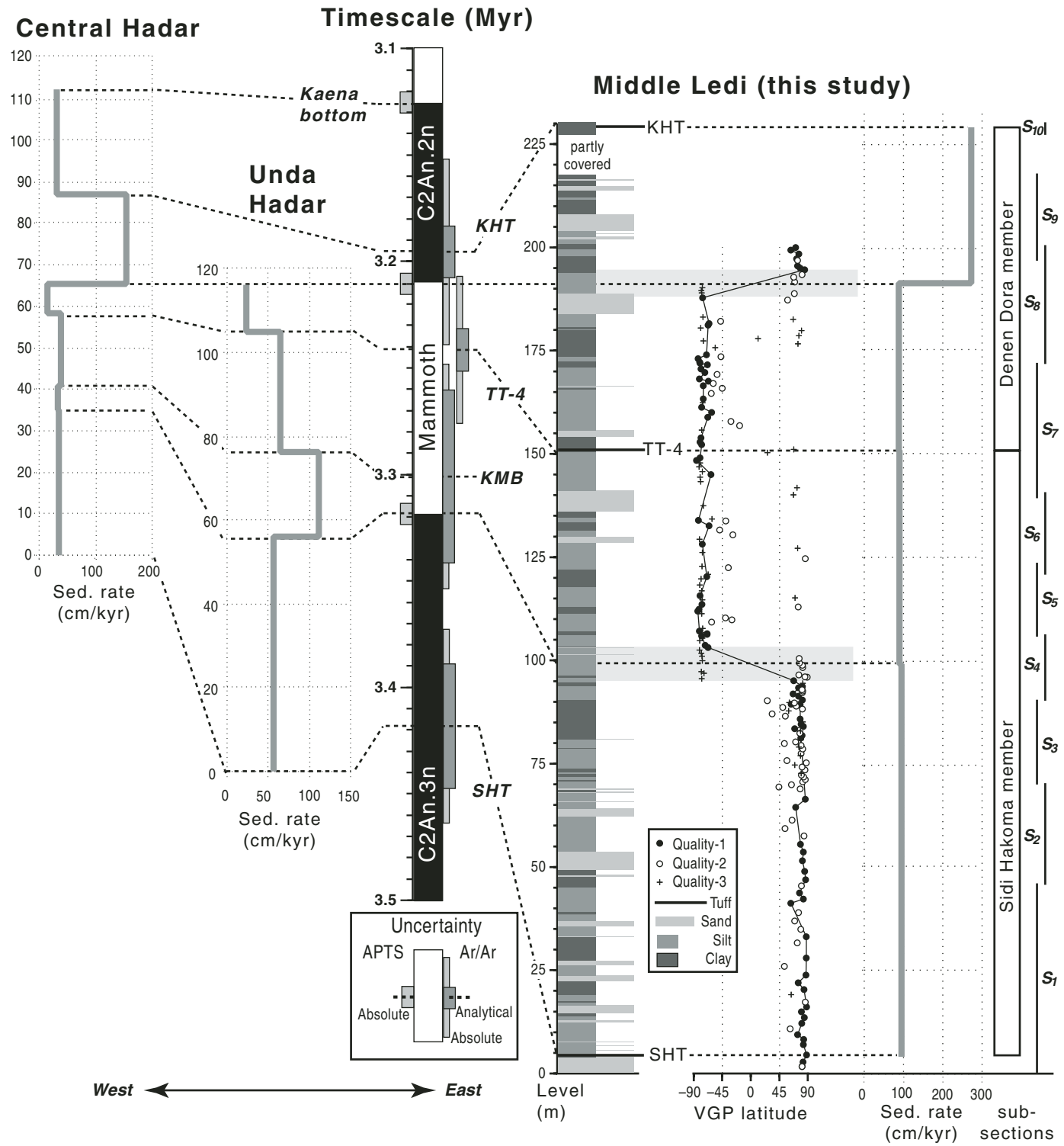

Figure 7. Middle Ledi section (right): Magnetostratigraphic results ("VGP latitude" is virtual geomagnetic pole latitude derived from characteristic remanent magnetization [ChRM] directions) with associated sediment accumulation rates (Sed. rate). Time scale (center): Correlations of tuffaceous and basaltic horizons (KHT—Kada Hadar Tuff, TT-4—Triple Tuff 4, KMB—Kada Damum Basalt, SHT—Sidi Hakoma Tuff) and chron boundaries to reference ages from calibrated $^{40}Ar/^{39}Ar$ dates on associated horizons and from the astronomically tuned polarity time scale (APTS), with their associated uncertainties (see Table 4). Unda Hadar and central Hadar (left): Stratigraphic levels of tuff horizons and chron boundaries and associated sediment accumulation rates from the Unda Hadar section (Renne et al., 1993) and the central Hadar section (Campisano, 2007) of the Hadar research area.

a tephra within the astronomically calibrated Gulf of Aden deposits (deMenocal and Brown, 1999). This slightly younger age is not significantly different from the $^{40}Ar/^{39}Ar$ result, but it provides a more precise age with lower absolute uncertainty. However, it should be noted that the tuning is based on the solution of Berger and Loutre (1991) not yet updated to the Laskar et al. (2004) solutions. A new age estimate for Triple Tuff-4 by Campisano (2007) of 3.256 ± 0.016 Ma is within one standard deviation of the previously reported Triple Tuff-4 age, but it suggests that Triple Tuff-4 could be slightly older. However, this estimate relies on only 10 single-crystal analyses in contrast to 20 single grains for Walter (1994). An independent check on age estimates of the Mammoth C2An.2r boundaries, the Sidi Hakoma Tuff, and the Triple Tuff-4 is provided later using our magnetostratigraphic results.

Sediment Accumulation Rates

For the five tie points provided by the three identified tuffaceous horizons and the two reversal boundaries of the Mammoth C2An.2r, the various proposed ages and associated uncertainties are plotted against stratigraphic level (Fig. 8).

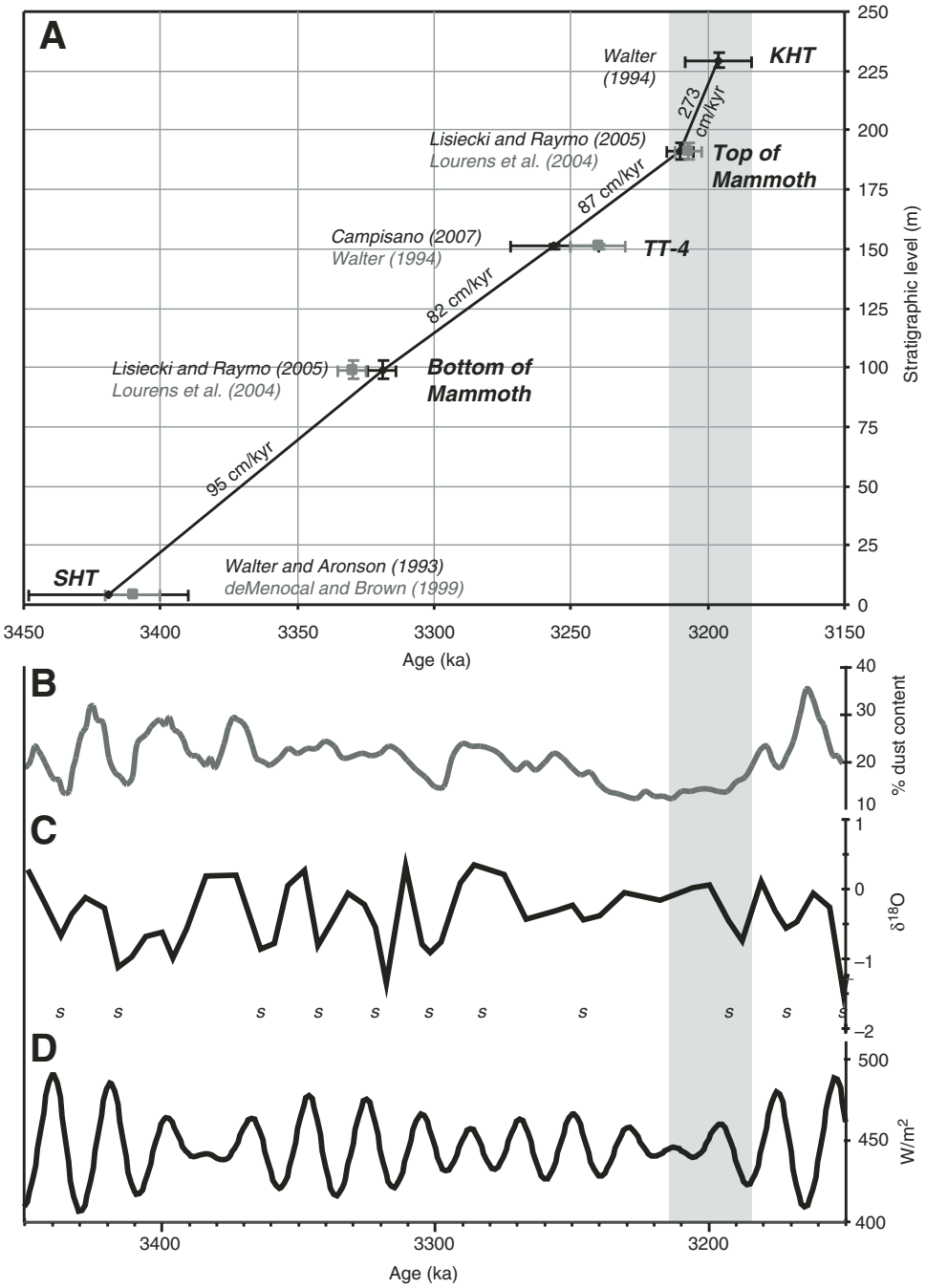

Figure 8. (A) Age versus stratigraphic level for the Middle Ledi section. Age estimates of tuffaceous horizons ($^{40}Ar/^{39}Ar$ date calibrated according to Renne et al. [1998] and given with 1σ error on age) are compared to chron boundary ages (from astronomically tuned polarity time scales with 5 k.y. estimated uncertainty on age) with associated uncertainties on stratigraphic position. KHT—Kada Hadar Tuff, TT-4—Triple Tuff 4, SHT—Sidi Hakoma Tuff. The best fit to constant sediment accumulation rates (indicated on the curve in cm/k.y.) is provided by age estimates depicted with black diamonds. Gray area indicates time span of the interval of high accumulation rate, which is compared to climate proxies and parameters: (B) Terrigenous dust off East Africa Deep Sea Drilling Project (DSDP) Site 721/722 (deMenocal, 1995), (C) Mediterranean planktonic $\delta^{18}O$ (Lourens et al., 1996) and sapropels (s) (Eimes et al., 2000), and (D) 21 June insolation at 11°N (Laskar et al., 2004).

Sediment accumulation rates are estimated by linear interpolation between the five successive tie points. An excellent linear fit is obtained below the top of the Mammoth C2An.2r down to the Sidi Hakoma Tuff. In this interval, interpolations of chron boundary ages fall within the analytical error of the $^{40}Ar/^{39}Ar$ ages. This supports the consistency between the calibrated $^{40}Ar/^{39}Ar$ ages (Renne et al., 1998) and the astronomically tuned polarity time scales (Lisiecki and Raymo, 2005; Lourens et al., 2005). The age estimates that minimize sediment accumulation rate variations are the Sidi Hakoma Tuff age of Walter and Aronson (1993), the Mammoth C2An.2r boundary ages of Lisiecki and Raymo (2005), and the Triple Tuff-4 age of Campisano (2007). Accordingly, rates are nearly constant (average 88 cm/k.y.) from the Sidi Hakoma Tuff at the base of the section to the top of the Mammoth C2An.2r, but a threefold increase (273 cm/k.y.) is indicated between the top of the Mammoth C2An.2r and the Kada Hadar Tuff (Table 4; Fig. 8).

This large increase in accumulation rates remains significant regardless of the proposed tie-point age estimate, and it is robust beyond uncertainties on ages and stratigraphic positions of reversals and tuffaceous horizons. Keeping the rate constant above the top of the Mammoth C2An.2r is not viable. It would require either an impossibly low stratigraphic position for the Kada Hadar Tuff at the 203 m level, or the unlikely option that the age of the Kada Hadar Tuff is too old by 3σ, even though this $^{40}Ar/^{39}Ar$ age with 26 sanidine analyses is one of the better constrained in the Hadar region (Walter, 1994). An error caused by invalid calibration of the fluence monitor standard is also unlikely because it would imply offsetting not only all the other otherwise concordant $^{40}Ar/^{39}Ar$ ages issued from the same laboratory conditions (i.e., the Berkeley Geochronology Center), but also the Sidi Hakoma Tuff astronomically calibrated in ocean records (deMenocal and Brown, 1999). Alternatively, constant rates would require shifting the age of the top of the Mammoth C2An.2r to a precession cycle older than reported. An error in the tuning of all the Mediterranean type sections (Lourens et al., 1996, 2005) and the 57 benthic $\delta^{18}O$ records (Lisiecki and Raymo, 2005) is unlikely. It would require not only changing the position of one precession cycle in these records, but also shifting positions of well-established 100 and 400 k.y. eccentricity cycles. Additionally, an error in the stratigraphic position of the paleomagnetic reversal in the type sections (e.g., through delayed acquisition of remanent magnetization) is unlikely given the detailed resolution of sampling and demagnetization of these sections (van Hoof and Langereis, 1991). Thus, we conclude from sediment accumulation rates in the Middle Ledi that deposition was near constant at ~90 cm/k.y. since ca. 3.4 Ma, and it increased significantly at ca. 3.2 Ma.

Comparison to Hadar Basin Stratigraphy

When compared to the Hadar and Gona areas, with typical 20–30 cm/yr accumulation rates (Campisano and Feibel, 2007; Quade et al., this volume), the ~90 cm/k.y. rates in the Ledi-Geraru area clearly indicate that it was positioned close to or within the depocenter of the Hadar Basin. When compared to the Unda Hadar (eastern) and central Hadar sections, an eastward thickening of the stratigraphy is immediately apparent (Fig. 7). The thickness between the Sidi Hakoma Tuff up to the top of the Mammoth C2An.2r in the central Hadar section is almost doubled in the Unda Hadar and more than tripled in the Middle Ledi. This eastward thickening is nearly identical among the central Hadar, Unda Hadar, and Middle Ledi sections at ~12 m/km (ratio of thickness increase in meters to E-W distance in kilometers between sections), and it translates into regional 1° easterly tilt of the Sidi Hakoma Tuff with respect to the horizon representing the top of the Mammoth C2An.2r.

Sediment accumulation rates derived between tie points compare well between the three sections (Fig. 7; Table 4). In the Unda Hadar, although the precise position of the Kada Hadar Tuff in relation to the top of the Mammoth interval is not readily available from published records, extrapolation of constant accumulation yields an unlikely stratigraphic position for the Kada Hadar Tuff (119.35 m) only a few meters above the Mammoth C2An.2r and much lower than the Confetti Clay horizon shown 15–25 m above the Mammoth C2An.2r in Schmitt and Nairn (1984). This strongly suggests that sediment accumulation must also have increased in this interval at Unda Hadar, because the Kada Hadar Tuff is only a few meters below the Confetti Clay (Campisano and Feibel, this volume). Below the Kada Hadar

TABLE 4. AGES, STRATIGRAPHIC LOCATIONS, AND ACCUMULATION RATES

Rock unit or reversal	Reference				Central Hadar		Unda Hadar		Middle Ledi	
	Age (ka)	±	δAge (ka)	ΔAge (ka)	Level (cm)	Rate (cm/k.y.)	Level (cm)	Rate (cm/k.y.)	Level (cm)	Rate (cm/k.y.)
SHT*	3419	±	43	45	0	–	0	–	432	–
Mam_b†	3319	±	5	5	3500	35	5600	56	9905	95
KMB§	3301	±	40	52	4081	32	7600	111	–	–
TT-4#	3256	±	16	36	5809	38	10,500	64	15,087	82
Mam_t†	3210	±	5	5	6509	15	11,600	24	19,111	87
KHT**	3196	±	12	43	8671	154	*11,935*	*extrapol.*	22,934	273
Kaena_b†	3127	±	5	5	11,201	37	–	–	–	–

Note: Reference ages of rock units are from: *—Walter and Aronson (1993), §—Renne et al. (1993), #—Campisano (2007), and **—Walter (1994). Reversal ages (_b and _t for chron bottom and top, respectively) are according to time scales of: †—Lisiecki and Raymo (2004). δAge—analytical error; ΔAge—absolute uncertainty; Level—stratigraphic levels, in italic if linearly extrapolated from rate at underlying tie point; Rate—sediment accumulation rate derived from linear interpolation.

Tuff, the chronostratigraphy at Hurda shows less constant rates (average of 64 cm/k.y.), possibly related to the larger uncertainty on the age of the Kada Damum Basalt (KMB) and on the reversals positions (using AF demagnetization only). In central Hadar, a pattern strikingly similar to that of the Middle Ledi is indicated by near constant rates (average of 30 cm/k.y.) from the Sidi Hakoma Tuff to the top of the Mammoth C2An.2r, followed by a fivefold increase (154 cm/k.y.) between the top of the Mammoth C2An.2r to the Kada Hadar Tuff. Interestingly, above the Kada Hadar Tuff, rates return to near average values (34 cm/k.y.) between the Kada Hadar Tuff and the base of the Kaena C2An.1r interval, indicating that the increase in accumulation rate was a short-lived event. Finally, the regional consistency of the results signifies that processes responsible for the accumulation increase operated at the scale of the entire Hadar Basin and cannot be attributed to inaccurate stratigraphic positions of reversals, to a local fault, or to a local change in the drainage pattern that would be restricted to only one section.

DISCUSSION

Tectonic Configuration of Hadar Basin

By extending the stratigraphic record further east into the Ledi-Geraru area, our results clearly show eastward thickening of the Hadar Formation. This result supports previous work that suggested thickening in eastward (Tiercelin, 1986) or northeastward (Wynn et al., 2006) directions (our results constrain the east-west component of thickening but not the north-south component). An eastward thickening pattern indicates that sediment accumulation space was more important on the eastern flank than on the western flank of the basin, suggesting an asymmetric eastward-tilting graben configuration. This basin geometry may have resulted from normal faulting on the eastern margin of the basin or eastward-increasing thermal subsidence (Einsele, 2000). We rule out the possibility that the dip formed before deposition to be later filled in by sediments because that would result in progradational stratigraphic successions (coarsening upward) in opposition to the observed aggradational patterns observed in the Hadar Formation.

To account for the observed 1° eastward dip accumulated in ~200 k.y. between the Sidi Hakoma Tuff and the top of Mammoth C2An.2r, significant subsidence is required toward the eastern margin of the basin (at least the ~300 m total thickness of the Hadar Formation). Normal faulting is present at the eastern end of the Ledi-Geraru research area. Basaltic lavas become progressively thicker and a more significant portion of the stratigraphy from west to east. Toward the west, the termination of these flows is expressed by an erosional escarpment defining the present irregular western edge of the Eibdaha Plateau because of their greater resistance to erosion (Fig. 1). Toward the east, these flows are cut by numerous north-south–trending normal faults. A major break (east of the Eibdaha Plateau) drops basalts with a thin Hadar sedimentary cover down to the west against the basalts to the east. This boundary continues to the south and is manifest as an ~50-m-high west-facing escarpment that we refer to as the Eibdaha fault zone. The Eibdaha fault zone forms the eastern boundary of the Hadar Formation stratigraphy, and the Eibdaha Plateau is tilted eastward both north and south of the Awash River. These relationships, observed in the field, on digital elevation models (90 m Shuttle Radar Topography Mission [SRTM] imagery), and on aerial photography, suggest a down-to-the-west normal displacement. However, the Eibdaha fault zone may postdate Hadar Formation deposition because it offsets the Hadar Formation, and rocks coeval with the Hadar Formation (Afar Stratoid Basalts) are exposed in the footwall (Kidane et al., 2003). Further investigation is required to constrain the age and displacement history on these faults.

Alternatively, the eastward thickness increase may result from increasing thermal subsidence, as suggested by the steadiness of the accumulation rates observed throughout the Hadar Basin during a relatively long time interval (ca. 3.4 Ma to ca. 3.2 Ma). We observe, however, that these rates (30–90 cm/k.y.) are greater than the low regional subsidence expected in the Pliocene by thermal and flexural modeling based on kinematic and crustal thickness reconstructions (Redfield et al., 2003). Redfield et al. (2003) estimated crustal thinning and thermal weakening at the scale of an entire 180-km-long "Hadar block" from the Ethiopian escarpment to the rift center since 20 Ma. In detail, Redfield et al. (2003) suggested that the logarithmic subsidence decrease since 6.2 Ma was negligible regionally, but that the elastic lithosphere became so thin that stretching accommodation was localized rather than regional. As a result, a high thermal gradient would be expected between the Ethiopian escarpment (elastic thickness up to 60 km) and the adjacent stretched lithosphere (elastic thickness down to 5 km). Consistently, the observed Hadar Formation thickening away from the Ethiopian escarpment may be related to the high gradient of flexural rigidity producing riftward downwarping through differential thermal subsidence, possibly enhanced by sediment loading as described on the western margin of the Afar Depression (Beyene and Abdelsalam, 2005), the Adama basin just south of the Afar Depression (Wolfenden et al., 2004), or the Gulf of Aden passive margin in Oman (Gunnell et al., 2007; Petit et al., 2007).

Interestingly, the observed sediment transport directions measured in the Hadar Formation are directed eastward, with proximal deposits (alluvial and fluvial sands and gravels) along the Ethiopian escarpment and distal lacustrine deposits toward the Afar Depression (Aronson and Taieb, 1981; Tiercelin, 1986; Quade et al., 2004). This suggests that the higher, eroding topography that provided the sediment source—such as the Ethiopian escarpment—was already present west of the basin as indicated by thermochronologic results from the Ethiopian Plateau (Pik et al., 2003; Gani et al., 2007). It should be noted that rift escarpments do not require active faulting to be sustained, but they are usually described as long-lasting (over 10s of m.y.) geomorphic features inherited from the main base-level drop of the initial rifting (e.g., Braun and van der Beek, 2004). We therefore argue that, although the Hadar Formation sediment originated from the

existing rift escarpment to the west, the accumulation was not primarily controlled by faulting along the rift escarpment but rather by increased subsidence toward the Afar Depression.

Environmental Change Ca. 3.2 Ma

The remarkably constant sediment accumulation rates from ca. 3.4 Ma to ca. 3.2 Ma suggest that the Hadar Basin was at close to dynamic aggradational equilibrium during that period. Perturbation of this steady state is required by the conspicuous sediment accumulation increase occurring between the top of the Mammoth C2An.2r interval and the Kada Hadar Tuff. Interestingly, the most distinctive sedimentologic feature of this particular interval in the Middle Ledi section is a 65% increase in the amount of sandstone. This increase is also noted at Hadar, where this interval includes a set of sandy layers referred to as the Denen Dora-2 and -3 sands (DD-2s, DD-3s). This interval has been intensely studied because it preserves a large proportion of the hominin fossil record from the Hadar Basin (Behrensmeyer, this volume). In addition to the large number of hominins from the DD-2 and DD-3 interval, this sequence also preserves by far the greatest number of paleontological specimens from Hadar. Of the 11 submember divisions at Hadar, specimens from the DD-2 and DD-3 submembers account for more than 40% of the Hadar paleontological assemblage but represent less than 8% of the time recorded (Campisano, 2007). Although the abundance of preserved specimens may be a result of ecological or taphonomic factors related to DD-2 and DD-3 depositional environments, it may also be a function of increased preservation potential associated with the exceptionally high rate of sediment deposition documented in this interval.

Whereas the DD-2 sand is laterally discontinuous and only 2.5 m in maximum thickness, the DD-3 sand is extensive and laterally persistent. This upward-fining sand can reach up to 10 m in thickness and displays an erosional base, well-developed cross-bedding, and lateral accretion surfaces (Tiercelin, 1986; Campisano and Feibel, this volume). The DD-3 forms a time-transgressive progradational sequence typical of a dissecting meandering fluvial system coming from the western Hadar region, where it is often conglomeratic (Quade et al., 2004). The sudden occurrence of this high-energy fluvial system prograding onto more distal sediments suggests three possible mechanisms forcing the drainage basin configuration: (1) water-level lowering, (2) decrease in basin subsidence, and/or (3) higher detrital influx (Keighley et al., 2003). At Hadar, the Kada Hadar Tuff is typically interbedded within the overbank silts of the DD-3 system and subsequently transitions to low-gradient fluvial, paludal, and lacustrine deposition similar to that found below the DD-3. This suggests that the basin quickly returned to dynamic equilibrium after the event, as also shown by a return to average values of accumulation rates in the central Hadar region (Campisano, 2007; Table 4).

For the Hadar Basin, variations in sediment accumulation rates have usually been attributed to tectonically controlled variations in accumulation space through fault-slip and subsidence (Aronson and Taieb, 1981; Tiercelin, 1986). Although this may be the case for the widespread ca. 2.9 Ma unconformity separating the Busidima and Hadar Formations (Quade et al., 2004), a major regional tectonic event at ca. 3.2 Ma, with associated long-term subsidence and uplift, can be ruled out by the sudden and short-lived nature of the observed accumulation increase. Also, increased subsidence would more likely result in transgression of distal sediments rather than the observed prograding DD-type sands. Taking the ages and associated uncertainties at face value, the accumulation increase found between the top of the Mammoth C2An.2r interval and the Kada Hadar Tuff would have occurred in less than 30 k.y. Within such a short time span, the basin can be assumed to have maintained steady-state conditions in relation to tectonic subsidence and relief. The observed accumulation increase and progradation of the DD sands are thus more likely related to landscape equilibration after (1) a sudden change in drainage configuration and/or (2) climatic fluctuations (Einsele and Hinderer, 1998). Deciding between these two possible causes is difficult. The drainage configuration may have been suddenly and significantly altered by mechanisms such as a regional tuff deposition, suddenly increasing erosional efficiency, or minor local faulting opening the basin outlet, draining the lake, and resulting in a base-level drop that could have induced increased sediment transport to the basin from up-river catchments. At present, no evidence for the occurrence of such mechanisms has been reported from the Hadar region. Alternatively, climatic fluctuations at or below the scale of precession cycles (20 k.y.) may have produced lowering of the lake level and/or increased erosional efficiency and sediment transport to the basin, without necessitating a change in drainage configuration.

This climate-related hypothesis, previously proposed for the DD-3 sand (Tiercelin, 1986), can be substantiated by comparison to existing climate proxies (Fig. 8). Locally, pollen and stable isotope analysis have been gathered from the Hadar Basin (Bonnefille et al., 2004; Levin et al., 2004; Quade et al., 2004; Wynn et al., 2006). However, the age resolution of these studies is still insufficient to decipher a short event at ca.3.2 Ma. Regionally relevant climate indicators are available with higher time resolution from the Gulf of Aden and the Mediterranean. They show that the ca. 3.2 Ma event occurs at the end of a relatively "quiet" period expressed by low variability in the amount of terrigenous material transported to the Gulf of Aden (deMenocal, 1995) as well as in Mediterranean planktonic $\delta^{18}O$ values (Lourens et al., 1996), and by fewer sapropel layers in the eastern Mediterranean basin (sapropel layers are tied to low-latitude summer insolation driving East African monsoon rainfall on the Ethiopian Highlands where both the Blue Nile and the Awash River originate; Emeis et al., 2000). This quiet period corresponds to a peculiar configuration in Earth's orbital parameters arising from a combination of low eccentricity and low-amplitude obliquity variation, reducing the precession influence on Earth insolation and favoring damped seasonality (Laskar et al., 2004). We propose that the ca. 3.2 Ma event may have been related to the onset of increased climate

variability, perturbing the landscape by increasing sediment discharge and increasing sediment accumulation after a relatively long period of low variability. Testing this hypothesis will require further work focusing on increasing temporal resolution of climatic proxies directly from the sediments of the Hadar Basin.

Relationship to Hominin Evolution and the Paleontological Record

The Hadar Basin contains abundant fossils of *Australopithecus afarensis* between 3.45 Ma and 2.95 Ma (Kimbel et al., 2004). These fossils sample an evolving lineage that can be traced back at least to the first appearance of an earlier species, *A. anamensis*, at ca. 4.2 Ma (Kimbel et al., 2006). Evolutionary changes occurred at various points in the *A. anamensis-afarensis* lineage. The last change was an increase in lower jaw size that probably indicates a general increase in body size (Lockwood et al., 2000; Kimbel et al., 2004). This increase in size took place at some point above the Kada Hadar Tuff (ca. 3.2 Ma) and before ca. 3.0 Ma, but the paucity of *A. afarensis* fossils between these ages makes it impossible to be more precise.

Among other mammalian fauna, there are an increase and influx of more arid-adapted taxa, particularly bovids, at Hadar during the interval of 3.2 Ma to 3.0 Ma (Campisano and Reed, 2007; Reed, 2008). The coincidence of a dramatic change in local rates of sediment accumulation with a shift in some records of global environmental change (discussed already) raises the possibility that the Afar faunal community was directly affected by these events. In particular, the onset of high-amplitude climate oscillations and increased aridity in eastern Africa between 3.15 and 2.95 Ma may have been linked to the size-related morphological changes within the *A. afarensis* lineage and the increasing proportion of more arid-adapted mammalian taxa during this period (Campisano and Feibel, 2007). These suggestions remain speculative, but they highlight the importance of well-calibrated records for fossils, chronology, and paleoenvironmental indicators to the study of variation within species as well as patterns of species turnover. In addition, more work is necessary in South Africa and other parts of the continent to determine whether the events in Hadar record are paralleled elsewhere.

ACKNOWLEDGMENTS

This work was funded by the Leakey Foundation, the Wenner Gren Foundation for Anthropological Research, the Institute of Human Origins, the School of Human Evolution and Social Change at Arizona State University, and the Netherlands Organisation for Scientific Research (NWO). Permission to conduct fieldwork was granted by the Authority for Research and Conservation of Cultural Heritage (of the Ethiopian Ministry of Youth, Sports, and Culture) with local permissions and assistance from the Culture and Tourism Bureau of the Afar Regional State government. We thank our field crew directed by Mesfin Mekonen, Bruno Paulet for help in the field and plane tickets, Klaudia Kuiper for $^{40}Ar/^{39}Ar$ issues, and Mark Dekkers and Andy Biggins for rock magnetic issues. Three anonymous reviews considerably improved the original manuscript, and we thank Jay Quade and Jonathan Wynn for their constructive comments.

REFERENCES CITED

Acton, G.D., Tessema, A., Jackson, M., and Bilham, R., 2000, The tectonic and geomagnetic significance of paleomagnetic observations from volcanic rocks from central Afar, Africa: Earth and Planetary Science Letters, v. 180, p. 225–241, doi: 10.1016/S0012-821X(00)00173-4.

Alemseged, Z., Spoor, F., Kimbel, W.H., Bobe, R., Geraads, D., Reed, D., and Wynn, J.G., 2006, A juvenile early hominin skeleton from Dikika, Ethiopia: Nature, v. 443, p. 296–301, doi: 10.1038/nature05047.

Aronson, J.A., and Taieb, M., 1981, Geology and paleogeography of the Hadar hominid site, Ethiopia, *in* Rapp, G., and Vondra, C.F., eds., Hominid Sites: Their Geologic Setting: Boulder, Colorado, Westview Press, p. 165–195.

Aronson, J.L., Schmitt, T.J., Walter, R.C., Taieb, M., Tiercelin, J.J., Johanson, D.C., Naeser, C.W., and Nairn, A.E.M., 1977, New geochronologic and palaeomagnetic data for the hominid-bearing Hadar Formation of Ethiopia: Nature, v. 267, p. 323–327, doi: 10.1038/267323a0.

Audin, L., Quidelleur, X., Coulie, E., Courtillot, V., Gilder, S., Manighetti, I., Gillot, P.Y., Tapponnier, P., and Kidane, T., 2004, Palaeomagnetism and K-Ar and Ar-40/Ar-39 ages in the Ali Sabieh area (Republic of Djibouti and Ethiopia): Constraints on the mechanism of Aden Ridge propagation into southeastern Afar during the last 10 Myr: Geophysical Journal International, v. 158, p. 327–345, doi: 10.1111/j.1365-246X.2004.02286.x.

Behrensmeyer, A.K., 2008, this volume, Paleoenvironmental context of the Pliocene A.L. 333 "First Family" Hominin Locality, Hadar Formation, Ethiopia, *in* Quade, J., and Wynn, J.G., eds., The Geology of Early Humans in the Horn of Africa: Geological Society of America Special Paper 446, doi: 10.1130/2008.2446(09).

Berger, A., and Loutre, M.F., 1991, Insolation values for the climate of the last 10,000,000 years: Quaternary Science Reviews, v. 10, p. 297–317, doi: 10.1016/0277-3791(91)90033-Q.

Besse, J., and Courtillot, V., 2002, Apparent and true polar wander and the geometry of the geomagnetic field in the last 200 million years: Journal of Geophysical Research, v. 107, doi: 10.1029/2000JB000050, 2300.

Beyene, A., and Abdelsalam, M.G., 2005, Tectonics of the Afar Depression: A review and synthesis: Journal of African Earth Sciences, v. 41, p. 41–59, doi: 10.1016/j.jafrearsci.2005.03.003.

Bonnefille, R., Potts, R., Chalie, F., Jolly, D., and Peyron, O., 2004, High-resolution vegetation and climate change associated with Pliocene *Australopithecus afarensis*: Proceedings of the National Academy of Sciences of the United States of America, v. 101, p. 12,125–12,129, doi: 10.1073/pnas.0401709101.

Braun, J., and van der Beek, P., 2004, Evolution of passive margin escarpments: What can we learn from low-temperature thermochronology?: Journal of Geophysical Research, v. 109, F04009, doi: 10.1029/2004JF000147.

Buddington, A.F., and Lindsley, D.H., 1964, Iron-titanium oxide minerals and synthetic equivalents: Journal of Petrology, v. 5, p. 310–357.

Campisano, C.J., 2007, Tephrostratigraphy and Hominin Paleoenvironments of the Hadar Formation, Afar Depression, Ethiopia [Ph.D. thesis]: New Brunswick, New Jersey, Rutgers, 601 p.

Campisano, C.J., and Feibel, C.S., 2007, Connecting local environmental sequences to global climate patterns: Evidence from the hominin-bearing Hadar Formation, Ethiopia: Journal of Human Evolution, v. 53, p. 515–527, doi: 10.1016/j.jhevol.2007.05.015.

Campisano, C.J., and Feibel, C.S., 2008, this volume, Depositional environments and stratigraphic summary of the Pliocene Hadar Formation at Hadar, Afar Depression, Ethiopia, *in* Quade, J., and Wynn, J.G., eds., The Geology of Early Humans in the Horn of Africa: Geological Society of America Special Paper 446, doi: 10.1130/2008.2446(08).

Campisano, C.J., and Reed, K.E., 2007, Spatial and temporal patterns of *Australopithecus afarensis* habitats at Hadar, Ethiopia: Philadelphia, Paleoanthropology Society Annual Meeting Abstracts, p. A6.

Clement, A.C., Hall, A., and Broccoli, A.J., 2004, The importance of precessional signals in the tropical climate: Climate Dynamics, v. 22, p. 327–341, doi: 10.1007/s00382-003-0375-8.

deMenocal, P.B., 1995, Plio-Pleistocene African Climate: Science, v. 270, p. 53–59, doi: 10.1126/science.270.5233.53.

deMenocal, P.B., 2004, African climate change and faunal evolution during the Pliocene-Pleistocene: Earth and Planetary Science Letters, v. 220, p. 3–24, doi: 10.1016/S0012-821X(04)00003-2.

deMenocal, P.B., and Brown, F.H., 1999, Pliocene tephra correlations between East African hominid localities, the Gulf of Aden and the Arabian Sea, *in* Agusti, J., Rook, L., and Andrews, P., eds., The Evolution of Terrestrial Ecosystems in Europe: Cambridge, Cambridge University Press, p. 23–54.

Dillon, M., and Franke, C., 2008, Diagenetic alteration of natural magnetic Fe-Ti oxides identified by energy dispersive spectroscopy (EDS) and low-temperature remanence and hysteresis measurements: Physics of the Earth and Planetary Interior, doi:10.1016/j.pepi.2008.08.003.

DiMaggio, E.N., Campisano, C.J., Arrowsmith, J R., Reed, K.E., Swisher, C.C., III, and Lockwood, C.A., 2008, this volume, Correlation and stratigraphy of the BKT-2 volcanic complex in west-central Afar, Ethiopia, *in* Quade, J., and Wynn, J.G., eds., The Geology of Early Humans in the Horn of Africa: Geological Society of America Special Paper 446, doi: 10.1130/2008.2446(07).

Dunlop, D., and Özdemir, Ö., 1997, Rock Magnetism: Fundamentals and Frontiers: Cambridge, Cambridge University Press, 573 p.

Einsele, G., 2000, Sedimentary Basins—Evolution, Facies, and Sediment Budget (2nd edition): Berlin, Springer-Verlag, 792 p.

Einsele, G., and Hinderer, M., 1998, Quantifying denudation and sediment-accumulation systems (open and closed lakes): Basic concepts and first results: Palaeogeography, Palaeoclimatology, Palaeoecology, v. 140, p. 7–21, doi: 10.1016/S0031-0182(98)00041-8.

Emeis, K.-C., Sakamoto, T., Wehausen, R., and Brumsack, H.-J., 2000, The sapropel record of the eastern Mediterranean Sea—Results of Ocean Drilling Program Leg 160: Palaeogeography, Palaeoclimatology, Palaeoecology, v. 158, p. 371–395, doi: 10.1016/S0031-0182(00)00059-6.

Franke, C., Frederichs, T., and Dekkers, M.J., 2007, Efficiency of heavy liquid separation to concentrate magnetic particles: Geophysical Journal International, doi: 10.1111/j.1365-246X.2007.03489.x, v. 170, p. 1053–1066.

Gani, N.D., Gani, M.R., and Abdelsalam, M.G., 2007, Blue Nile incision on the Ethiopian Plateau: Pulsed plateau growth, Pliocene uplift, and hominin evolution: GSA Today, v. 17, no. 9, p. 4–11, doi: 10.1130/GSAT01709A.1.

Gunnell, Y., Carter, A., Petit, C., and Fournier, M., 2007, Post-rift seaward downwarping at passive margins: New insights from southern Oman using stratigraphy to constrain apatite fission-track and (U-Th)/He dating: Geology, v. 35, p. 647–650, doi: 10.1130/G23639A.1.

Hailemichael, M., Aronson, J.L., Savin, S., Tevesz, M.J.S., and Carter, J.G., 2002, $\delta^{18}O$ in mollusk shells from Pliocene Lake Hadar and modern Ethiopian lakes: Implications for history of the Ethiopian monsoon: Palaeogeography, Palaeoclimatology, Palaeoecology, v. 186, p. 81–99, doi: 10.1016/S0031-0182(02)00445-5.

Hart, W.K., Walter, R.C., and WoldeGabriel, G., 1992, Tephra sources and correlations in Ethiopia: Application of elemental and neodymium isotope data: Quaternary International, v. 13–14, p. 77–86, doi: 10.1016/1040-6182(92)90012-Q.

Hilgen, F.J., 1991, Astronomical calibration of Gauss to Matuyama sapropels in the Mediterranean and implication for the geomagnetic polarity time scale: Earth and Planetary Science Letters, v. 104, p. 226–244, doi: 10.1016/0012-821X(91)90206-W.

Johanson, D.C., and Taieb, M., 1976, Plio-Pleistocene hominid discoveries in Hadar, Ethiopia: Nature, v. 260, p. 293–297, doi: 10.1038/260293a0.

Johanson, D.C., Taieb, M., and Coppens, Y., 1982, Pliocene hominids from the Hadar Formation, Ethiopia (1973–1977): Stratigraphic, chronological, and paleoenvironmental contexts, with notes on hominid morphology and systematics: American Journal of Physical Anthropology, v. 57, p. 373–402, doi: 10.1002/ajpa.1330570402.

Kakol, Z., Sabol, J., Kozlowski, A., and Honig, J.M., 1994, Influence of titanium doping on the magnetocrystalline anisotropy of magnetite: Physical Review B: Condensed Matter and Materials Physics, v. 49, p. 12,767–12,772.

Keighley, D., Flint, S., Howell, J., and Moscariello, A., 2003, Sequence stratigraphy in lacustrine basins: A model for part of the Green River Formation (Eocene), southwest Uinta Basin, Utah: Journal of Sedimentary Research, v. 73, p. 987–1006, doi: 10.1306/050103730987.

Kidane, T., Courtillot, V., Manighetti, I., Audin, L., Lahitte, P., Quidelleur, X., Gillot, P.Y., Gallet, Y., Carlut, J., and Haile, T., 2003, New paleomagnetic and geochronologic results from Ethiopian Afar: Block rotations linked to rift overlap and propagation and determination of a similar to 2 Ma reference pole for stable Africa: Journal of Geophysical Research–Solid Earth, v. 108, doi: 10.1029/2001JB000645.

Kimbel, W.H., Rak, Y., and Johanson, D.C., 2004, The Skull of *Australopithecus afarensis*: New York, Oxford University Press, 254 p.

Kimbel, W.H., Lockwood, C.A., Ward, C.V., Leakey, M.G., Rak, Y., and Johanson, D.C., 2006, Was *Australopithecus anamensis* ancestral to *A. afarensis*? A case of anagenesis in the hominin fossil record: Journal of Human Evolution, v. 51, p. 134–152, doi: 10.1016/j.jhevol.2006.02.003.

Kirschvink, J.L., 1980, The least-square line and plane and the analysis of paleomagnetic data: Geophysical Journal of the Royal Astronomical Society, v. 62, p. 699–718.

Krása, D., Shcherbakov, V.P., Kunzmann, T., and Petersen, N., 2005, Self-reversal of remanent magnetization in basalts due to partially oxidized titanomagnetites: Geophysical Journal International, v. 162, p. 115–136, doi: 10.1111/j.1365-246X.2005.02656.x.

Kuiper, K.F., Hilgen, F.J., Steenbrink, J., and Wijbrans, J.R., 2004, $^{40}Ar/^{39}Ar$ ages of tephras intercalated in astronomical tuned Neogene sedimentary sequences in the eastern Mediterranean: Earth and Planetary Science Letters, v. 222, p. 583–597, doi: 10.1016/j.epsl.2004.03.005.

Lahitte, P., Gillot, P.Y., Kidane, T., Courtillot, V., and Bekele, A., 2003, New age constraints on the timing of volcanism in central Afar, in the presence of propagating rifts: Journal of Geophysical Research, v. 108, doi: 10.1029/2001JB001689, 2123.

Laskar, J., Robutel, P., Joutel, F., Gastineau, M., Correia, A.C.M., and Levrard, B., 2004, A long-term numerical solution for the insolation quantities of the Earth: Astronomy and Astrophysics, v. 428, doi: 10.1051/0004-6361:20041335, p. 261–285.

Levin, N.E., Quade, J., Simpson, S.W., Semaw, S., and Rogers, M., 2004, Isotopic evidence for Plio-Pleistocene environmental change at Gona, Ethiopia: Earth and Planetary Science Letters, v. 219, p. 93–110, doi: 10.1016/S0012-821X(03)00707-6.

Lisiecki, L.E., and Raymo, M.E., 2005, A Pliocene-Pleistocene stack of 57 globally distributed benthic $\delta^{18}O$ records: Paleoceanography, v. 20, p. PA1003, doi: 10.1029/2004PA001071.

Lockwood, C.A., Kimbel, W.H., and Johanson, D.C., 2000, Temporal trends and metric variation in the mandibles and teeth of *Australopithecus afarensis*: Journal of Human Evolution, v. 39, p. 23–55, doi: 10.1006/jhev.2000.0401.

Lourens, L.J., Antonarakou, A., Hilgen, F.J., Van Hoof, A.A.M., Vergnaud Grazzini, C., and Zachariasse, W.J., 1996, Evaluation of the Plio-Pleistocene astronomical timescale: Paleoceanography, v. 11, p. 391–413.

Lourens, L.J., Wehausen, R., and Brumsack, H.J., 2001, Geological constraints on tidal dissipation and dynamical ellipticity of the Earth over the past three million years: Nature, v. 409, p. 1029–1033, doi: 10.1038/35059062.

Lourens, L.J., Hilgen, F.J., Laskar, J., Shackelton, N.J., and Wilson, D.S., 2004, The Neogene Period, *in* Gradstein, F.M., Ogg, J.G., and Smith, A.G., eds., A Geologic Time Scale 2004: Cambridge, Cambridge University Press, p. 409–440.

Manighetti, I., Tapponnier, P., Courtillot, V., Gallet, Y., Jacques, E., and Gillot, P.Y., 2001, Strain transfer between disconnected, propagating rifts in Afar: Journal of Geophysical Research–Solid Earth, v. 106, p. 13,613–13,665, doi: 10.1029/2000JB900454.

McFadden, P.L., and McElhinny, M.W., 1988, The combined analysis of remagnetization circles and direct observations in palaeomagnetism: Earth and Planetary Science Letters, v. 87, p. 161–172, doi: 10.1016/0012-821X(88)90072-6.

Petit, C., Fournier, M., and Gunnell, Y., 2007, Tectonic and climatic controls on rift escarpments: Erosion and flexural rebound of the Dhofar passive margin (Gulf of Aden, Oman): Journal of Geophysical Research, v. 112, B03406, doi: 10.1029/2006JB004554.

Pik, R., Marty, B., Carignan, J., and Lave, J., 2003, Stability of the Upper Nile drainage network (Ethiopia) deduced from (U-Th)/He thermochronometry: Implications for uplift and erosion of the Afar plume dome: Earth and Planetary Science Letters, v. 215, p. 73–88, doi: 10.1016/S0012-821X(03)00457-6.

Quade, J., Levin, N., Semaw, S., Stout, D., Renne, P., Rogers, M., and Simpson, S., 2004, Paleoenvironments of the earliest stone toolmakers, Gona, Ethiopia: Geological Society of America Bulletin, v. 116, p. 1529–1544, doi: 10.1130/B25358.1.

Quade, J., Levin, N.E., Simpson, S.W., Butler, R., McIntosh, W.C., Semaw, S., Kleinsasser, L., Dupont-Nivet, G., Renne, P., and Dunbar, N., 2008, this volume, The geology of Gona, Afar, Ethiopia, *in* Quade, J., and Wynn, J.G., eds., The Geology of Early Humans in the Horn of Africa: Geological Society of America Special Paper 446, doi: 10.1130/2008.2446(01).

Redfield, T.F., Wheeler, W.H., and Often, M., 2003, A kinematic model for the development of the Afar Depression and its paleogeographic implications: Earth and Planetary Science Letters, v. 216, p. 383–398, doi: 10.1016/S0012-821X(03)00488-6.

Reed, K.E., 2008, Paleoecological patterns at the Hadar hominin site, Afar Regional State, Ethiopia: Journal of Human Evolution, v. 54, no. 6, p. 743–768.

Renne, P.R., Walter, R.C., Verosub, K.L., Sweitzer, M., and Aronson, J.L., 1993, New data from Hadar (Ethiopia) support orbitally tuned time scale to 3.3 Ma: Geophysical Research Letters, v. 20, p. 1067–1070, doi: 10.1029/93GL00733.

Renne, P.R., Swisher, C.C., III, Deino, A.L., Karner, D.B., Owens, T.L., and DePaolo, D.J., 1998, Intercalibration of standards, absolute ages and uncertainties in $^{40}Ar/^{39}Ar$ dating: Chemical Geology, v. 145, p. 117–152, doi: 10.1016/S0009-2541(97)00159-9.

Renne, P.R., WoldeGabriel, G., Hart, W.K., Heiken, G., and White, T.D., 1999, Chronostratigraphy of the Mio-Pliocene Sagantole Formation, middle Awash Valley, Afar Rift, Ethiopia: Geological Society of America Bulletin, v. 111, p. 869–885, doi: 10.1130/0016-7606(1999)111<0869:COTMPS>2.3.CO;2.

Schmitt, T.J., and Nairn, A.E.M., 1984, Interpretations of the magnetostratigraphy of the Hadar hominid site: Ethiopia, v. 309, p. 704–706.

Sepulchre, P., Ramstein, G., Fluteau, F., Schuster, M., Tiercelin, J.J., and Brunet, M., 2006, Tectonic uplift and eastern Africa aridification: Science, v. 313, p. 1419–1423, doi: 10.1126/science.1129158.

Spiegel, C., Kohn, B.P., Belton, D.X., and Gleadow, A.J.W., 2007, Morphotectonic evolution of the central Kenya rift flanks: Implications for late Cenozoic environmental change in East Africa: Geology, v. 35, p. 427–430, doi: 10.1130/G23108A.1.

Taieb, M., Johanson, D.C., Coppens, Y., and Aronson, J.L., 1976, Geological and palaeontological background of Hadar hominid site, Afar, Ethiopia: Nature, v. 260, p. 289–293, doi: 10.1038/260289a0.

Tamrat, E., Thouveny, N., and Taieb, M., 1996, Magnetostratigraphy of the lower member of the Hadar Formation (Ethiopia): Evidence for a short normal event in the mammoth subchron: Studia Geophysica et Geodaetica, v. 40, p. 313–335, doi: 10.1007/BF02300746.

Tauxe, L., 1998, Paleomagnetic Principles and Practice: Dordrecht, Kluwer Academic Publisher, 299 p.

Tauxe, L., 2005, Inclination flattening and the geocentric axial dipole hypothesis: Earth and Planetary Science Letters, v. 233, p. 247–261, doi: 10.1016/j.epsl.2005.01.027.

Thurmond, A.K., Abdelsalam, M.G., and Thurmond, J.B., 2006, Optical-radar-DEM remote sensing data integration for geological mapping in the Afar Depression, Ethiopia: Journal of African Earth Sciences, v. 44, p. 119–134, doi: 10.1016/j.jafrearsci.2005.10.006.

Tiercelin, J.J., 1986, The Pliocene Hadar Formation, Afar Depression of Ethiopia, *in* Frostick, L.E., Renaut, R.W., Reid, I., and Tiercelin, J.J., eds., Sedimentation in the African Rifts: Oxford, Blackwell Scientific, p. 221–240.

Ukstins, I.A., Renne, P.R., Wolfenden, E., Baker, J., Ayalew, D., and Menzies, M., 2002, Matching conjugate volcanic rifted margins: $^{40}Ar/^{39}Ar$ chronostratigraphy of pre- and syn-rift bimodal flood volcanism in Ethiopia and Yemen: Earth and Planetary Science Letters, v. 198, p. 289–306, doi: 10.1016/S0012-821X(02)00525-3.

Valet, J.-P., Meynadier, L., and Guyodo, Y., 2005, Geomagnetic dipole strength and reversal rate over the past two million years: Nature, v. 435, p. 802–805, doi: 10.1038/nature03674.

Vandamme, D., 1994, A new method to determine paleosecular variation: Physics of the Earth and Planetary Interiors, v. 85, p. 131–142, doi: 10.1016/0031-9201(94)90012-4.

van Hoof, A.A.M., and Langereis, C.G., 1991, Reversal records in marine marls and delayed acquisition of remanent magnetization: Nature, v. 351, p. 223–224, doi: 10.1038/351223a0.

Walter, R.C., 1994, Age of Lucy and the First Family: Single-crystal $^{40}Ar/^{39}Ar$ dating of the Denen Dora and lower Kada Hadar Members of the Hadar Formation: Geology, v. 22, p. 6–10, doi: 10.1130/0091-7613(1994)022<0006:AOLATF>2.3.CO;2.

Walter, R.C., and Aronson, J.L., 1993, Age and source of the Sidi Hakoma Tuff, Hadar Formation, Ethiopia: Journal of Human Evolution, v. 25, p. 229–240, doi: 10.1006/jhev.1993.1046.

Wolfenden, E., Ebinger, C., Yirgu, G., Deino, A., and Ayalew, D., 2004, Evolution of the northern Main Ethiopian Rift: Birth of a triple junction: Earth and Planetary Science Letters, v. 224, p. 213–228, doi: 10.1016/j.epsl.2004.04.022.

Wynn, J.G., Alemseged, Z., Bobe, R., Geraads, D., Reed, D., and Roman, D.C., 2006, Geological and palaeontological context of a Pliocene juvenile hominin at Dikika, Ethiopia: Nature, v. 443, p. 332–336, doi: 10.1038/nature05048.

Wynn, J.G., Roman, D.C., Alemseged, Z., Reed, D. Geraads, D., and Munro, S., 2008, Stratigraphy, depositional environments, and basin structure of the Hadar and Busidima Formations at Dikika, Ethiopia, *in* Quade, J., and Wynn, J.G., eds., The Geology of Early Humans in the Horn of Africa: Geological Society of America Special Paper 446, doi: 10.1130/2008.2446(04).

Yemane, T., 1997, Stratigraphy and Sedimentology of the Hadar Formation [Ph.D. thesis]: Ames, Iowa State University, 182 p.

Manuscript Accepted by the Society 17 June 2008